INTERFACIAL SHEAR MODELING AND FLOW PREDICTIONS FOR INTERNAL FLOWS OF PURE VAPOR EXPERIENCING FILM CONDENSATION

By

A. Narain

IMA Preprint Series # 1103

January 1993

INTERFACIAL SHEAR MODELING AND FLOW PREDICTIONS FOR INTERNAL FLOWS OF PURE VAPOR EXPERIENCING FILM CONDENSATION

A. Narain
Department of Mechanical Engineering and Engineering Mechanics
Michigan Technological University
Houghton, MI 49931

TABLE OF CONTENTS

ABSTRACT

Internal flow of pure vapor experiencing film condensation on the walls of a straight horizontal duct is studied. The commonly occurring *annular* case of turbulent (or laminar) vapor flow in the core and laminar flow of the liquid condensate—with or without waves on the interface—is emphasized.

We propose and implement a new methodology which models interfacial shear with the help of first-principles based theory, computations, and reliable experimental data on heat transfer rates. Other details of the flow are predicted with the help of this model. These predictions are shown to be in agreement with relevant experimental data. Correlations for film thickness, heat transfer rates, and pressure drops are also given.

NOMENCLATURE

This is a partial list of significant variables used in the paper.

h	Gap between the plates (see Figure 1), m
(x,y)	Physical distances along and across the horizontal plate, (m, m)
(x,y)	Non-dimensional values of (x,y) as defined in equation (2)
U	Physical value of the average vapor speed at the inlet, m/s
k	Thermal conductivity, W/(m-K)
C_p	Specific heat, J/(Kg-K)
p	Pressure, N/m^2
p_o	Pressure at the inlet, N/m^2
(u,v)	Values of x and y components of velocity, m/s
(u,v)	Non-dimensional values of velocity components u and v as defined in equation (2)
$\mathcal{T}$	Temperatures, K
$\Delta\mathcal{T}$	Temperature difference between the vapor and the wall, K or ^oC
T	Non-dimensional temperatures as defined in (2)
$\dot{m}$	Non-dimensional value of local condensation rate, here $\dot{m} \equiv \dot{m}/\rho_1 U$, where $\dot{m}$ is the actual condensation rate in Kg/ (m^2-s) at the interface
h_{fg}	Latent heat (h_g-h_f), J/Kg
Ja	Jacob number, $C_{p1}\Delta\mathcal{T}/h_{fg}$
Re	Reynolds numbers as defined in (7)
Re_{in}	Inlet Reynolds number ($\rho_2 Uh/\mu_2$)

$\bar{h}_x$ Average heat transfer coefficient over length x of the bottom plate

Greek Symbols

p Subscripted physical pressures

π_I Non-dimensional pressures as defined in equation (2)

π (x) Non-dimensional pressure π_2 in the vapor phase

ρ Density, Kg/m^3

μ Viscosity, Pa-s

ν Kinematic Viscosity, m^2/s

α Thermal diffusivity, m^2/s

Δ Physical value of condensate thickness, m

δ Non-dimensional value of condensate thickness

Subscripts

I It takes a value of 1 or 2

1 Liquid Phase

2 Vapor Phase

s Saturation condition

w Wall

1. INTRODUCTION AND BACKGROUND

There is a substantial body of scientific literature with regard to film condensation of vapors on surfaces. Here we briefly, and therefore not comprehensively, outline the existing knowledge base and how they relate to this paper. For convenience, we describe the background knowledge in the following categories (a)-(f):

(a) Studies of relevant film condensation problems

Classical results of Nusselt [1] and Rohsenow [2] dealt with film condensation of stationary vapor on cold surfaces. Subsequently a significant amount of analytical and experimental studies dealt with condensation of flowing vapor on horizontal or vertical plates ([3], [4], [5], [6], [7], etc.), over cylinders ([5], [8], etc.), inside pipes ([9], [10], etc.), between parallel plates ([11], [12]), inside annular passages ([13], etc.), over drops ([14]), etc. We investigate here, because of the availability of reliable experimental data [15], film condensation flow between horizontal parallel plates (see Figure 1). This flow situation is an approximate model for the experimental situation of flow in a horizontal duct of rectangular cross-section. However the method and results given in this paper are of general value because they can be adapted for a study of condensing flows in *any* straight duct.

(b) First principle and model equations

With regard to equations modeling film condensation, the knowledge base is rigorous and well established (see Delhaye [16] and Ishii [17]). Note, however, that the simpler equations used by Nusselt [1], Sparrow and Gregg [3], Shekriladze and Gomelauri [5], etc. remain valid approximate equations in the context of their respective problems. However, there are two open issues. The first issue relates to a lack of a general framework (see Carey [18]) on how to use non-equilibrium thermodynamics towards determining the temperature difference across a very thin vapor liquid phase change zone, adequately modeled here as a sharp interface. This issue is not relevant because experimental evidence, as pointed out by Rohsenow [19], indicates that for non-metallic vapors—situations of concern here—the temperature difference across the interface is negligible and it is reasonable to assume that both sides of the interface are at equilibrium saturation temperature determined by the local pressure. The second open issue regarding the state of knowledge of interfacial shear models is addressed in this paper and is described below.

(c) Relevant interfacial shear models

An appropriate physical model for interfacial shear, in combination with the governing equations for the flow, can completely predict most of the details of condensing flows. For estimating interfacial shear on the condensate, some of the practices have been:

i. to use friction factor models as if the gas was flowing over an impermeable wall [13];
ii. to use Lockhart-Martinelli [20] type correlations and to attempt to relate it to condensation [21];
iii. to account for the significant effects of vapor-suction at the interface with the help of any one or more of the following models: Shekriladze and Gomelauri [5] model, theoretical results of Kinney and Sparrow [22], and film models proposed by Mickley [23];

iv. to account for interfacial waves through Wallis type correlation [24] or Nikuradse type equation in terms of an effective roughness [25].

However all of the above models, when used for flow between parallel plates, yield results which are in poor quantitative agreement with reliable experimental measurements (e.g., see Figure 5) on film thickness and heat transfer rates. A recognition of the importance of interfacial shear and some understanding of its influence on film condensation does however exist in the works of Rohsenow, et al. [26], Dukler [27], Blangetti [28], Chen et al.[29], etc. and is coherently discussed in the book of Stephan [30]. There is still, however, a great need for a general and rigorous framework for development of interfacial shear models whose predictions of condensing flows are in agreement with experiments.

(d) Fundamental fluid dynamical issues and their relation to interfacial shear models for film condensation flows.

The following issues are relevant to understanding interfacial shear models:

i. Flow regime maps ([31], [32]) for two phase duct flows, with or without phase change, are significant as various gas-liquid configurations are possible in the flow. Despite this, for some very practical ranges of inlet vapor mass flux $\dot{M}\,(0 \le \dot{M} \le \dot{M}_{cr})$ and temperature difference $\Delta\mathcal{T}$ ($0 \le \Delta\mathcal{T} \le \Delta\mathcal{T}_{crit}$) between the vapor and the condensing surface, stable film condensation flows (with or without interfacial waves) are observed on earth over sufficient lengths ($L \le L_{crit}$) of horizontal [15] or vertical ducts. This paper confines itself to this commonly occurring *annular* regime. The interface here is not active in the sense of continuous droplet formation and their deposition as seen in some *wispy annular* two phase flows ([18], [25]).

ii. Role of vapor-suction at the interface is significant for condensing flows. In classical fluid mechanics, flow over an impermeable wall has much lower wall shear than flow over a wall with suction (see Schlichting [33], p.368). This is because, in flows with suction, a fluid element *slightly above* the plate moves forward with a significant speed. However, at some distance downstream it gets *drawn* to the plate where its forward speed reduces to zero. This, as compared to flow over an impermeable wall, leads to larger decelerations and hence much larger retarding forces and accompanying larger wall shear stress. This suction effect continues to be significant for film condensation flows because the flow of liquid condensate is usually much more sluggish than the vapor flow. The sluggishness is due to the thinness of the film as it flows over a stationary surface and, usually, significantly higher density of the condensate.

iii. The shear stresses induced by a vapor flow which is turbulent slightly above the interface is likely to have a different form of dependence on flow variables than shear stresses which are caused by a vapor flow which is entirely laminar.

iv. The interfacial shear for turbulent vapor is expected to be significantly affected by whether the interface is smooth or has an effective roughness in the form of waves. Experiments ([15]) indicate that for a given temperature difference $\Delta\mathcal{T}$ between the vapor and the wall, there is an inlet vapor speed up to which a film is smooth over a given length of the duct. After this speed, two dimensional waves appear on the downstream side of the duct. Eventually a speed is reached

when all of the condensate is *wavy* with a steady three dimensional pattern which *may* be viewed as an effective roughness. A depiction of the wave patterns for condensing flows is given in Figures 6.1-6.2 of [15] and it is similar to the wave patterns for air-water flows given in Figure 14.12 of [34] (p. 483).

v. Condensing flows can have liquid film flows which are smooth *and* laminar, or wavy *and* laminar, or wavy *and* turbulent. For flows investigated in this paper, the condensate was always laminar. This is because the *condensate Reynolds number* (see [18], p. 370) was always less than 1600. However, for gravity driven condensate flows in vertical pipes, the study of flow situations involving turbulent condensate is relevant over certain downstream distances and are discussed in [27] and [28]. This paper focuses on the smooth or wavy regimes of *laminar* condensates alone.

vi. For flow of a single fluid in a duct at a specified average speed, the wall shear variations for a flow which is fully developed at the inlet is different from a developing flow for which the inlet velocity profile is uniform. Because of dominance of interfacial shear (due to suction or waviness effects) in film condensation flows, we show in this paper that this type of variation in inlet flow condition usually has no significant effect on the values of interfacial shear and condensate thickness.

vii. If noncondensible gaseous impurities are present, they tend to concentrate at the interface and set up diffusion processes which usually lead to significant reduction in heat transfer rates ([35], [36], etc.). This phenomenon and its impact on interfacial shear is not investigated here because we focus exclusively on *pure* vapors.

(e) <u>Currently available tools for modeling or analysis and the significance of the proposed method.</u>

The current status of a complete numerical solution of this type of non-linear free boundary problem is inadequate because of problems with numerical convergence and numerical stability. This is why relevant studies ([37]) usually exclude handling of actual interface conditions for condensing flows. However, in principle, for laminar flow of vapor *and* laminar condensate, full computational simulation of film condensation flows is possible. For turbulent flows of vapor (with smooth or wavy interface), a numerical solution would require use of turbulence models which are, first of all, able to handle interface conditions and, secondly, able to predict friction factors in agreement with the known empirical models for single phase flows ([38]) or condensing flows (such as the one proposed here). This type of knowledge of turbulence models, and computational ability to use them to predict film condensation flows, is not yet available.

Recall that despite the status of turbulence modeling at the time of Moody's celebrated work [38], he was able to predict wall shear for fully developed turbulent flow of a single fluid in a pipe by combining reliable experimental measurements, an overall momentum balance, and proper non-dimensionalization. This paper provides a similar approach, in terms of underlying philosophy, for modeling interfacial shear in internal condensing flows.

Here we develop a first-principles based solution scheme for local variations in the lower

dimensional unknowns (film thickness, average vapor speed, etc.) which allows for *any* admissible model of friction factor at the interface. We define, for the first time, this "admissible class." The correct estimate for interfacial shear is then obtained by *finding* the model which predicts the lower dimensional unknowns (film thickness, heat transfer rate, etc.) in good agreement with reliable experimental data. This method is applied to the flow in Figure 1 to obtain models for interfacial shear.The models are then used to predict and understand other details of condensing flows.

(f) Relation to the existing knowledge-base of heat transfer correlations.

The primary interest in condensing flows is due to the large amount of latent heat that can be removed from condensing flows. Therefore a significant amount of reasonably good empirical and semi-empirical heat transfer correlations ([13], [39], [40], [41], [42], etc.) exist for such flows.

Average heat transfer coefficients, heat removed per unit area per unit temperature difference between the vapor and the condensing surface, is not likely to vary much with the geometry of a duct if the average speed of the vapor above the condensing surface is approximately the same. Because of this, Lu found (see Fig. 6.41of [15]) that his experimental data are in reasonable agreement (within $\pm$ 25%) with correlations of Soliman, Schuster, and Berenson [13], Shah [42], and his own (given as (6.20) and (6.22) on pp. 6.67-6.70 of [15]). Because of this general agreement, its reliability, and its relevance to our geometry, we use here the data of Lu [15]. Also note that with the exception of heat transfer correlations of the type given by Lu [15], or correlations given in this paper, most of the other correlations are not *directly usable* because they merely relate heat transfer rates to some other unknowns (such as quality, etc.) of the flow.

Lu [15] also attempts to predict heat transfer rates from an interfacial shear model and a system of governing equations which do not include the vapor momentum balance. As a result his model for interfacial shear (see Figure 7) is inconsistent with the complete set of governing equations *needed* to model the physics of the flow. Therefore, there continues to be a need to develop a model for interfacial shear. This paper addresses this need within a specified range of flow parameters. Furthermore we give a general method which, in conjunction with additional experiments, can be used to extend the range of flow parameters beyond what is considered here.

2. MODEL EQUATIONS AND NON-DIMENSIONAL PARAMETERS FOR FLOW BETWEEN PARALLEL PLATES

After scaling approximations for the shear dominated steady flow in Figure 1, the general equations reduce to the commonly used ([3], [4], etc.) forms given in this section. The general equations are available, among many places ([16], [17], etc.), in Narain and Kizilyalli (equations (1) to (9) of [11]), and the scaling assumptions are given in Chen and Kocamustafaogullari [10] or Narain and Kizilyalli [11].

We denote the liquid and vapor phases in the flow of Figure 1 by a subscript I: I = 1 for liquid and I = 2 for vapor. We represent the fluid properties by their representative constant values for each phase (I = 1 or 2). Let ρ_I be the densities, k_I be the thermal conductivities, μ_I be the viscosities, and C_{pI} be the specific heats. For the flow variables, let $\mathcal{T}_I$ be the temperature fields, p_I be the pressure fields, $\mathcal{T}_s$ (p) be the saturation temperature of the vapor as a function of the pressure p, Δ be the film thickness, and

$$\mathbf{v}_I = u_I\mathbf{i} + v_I\mathbf{j} \tag{1}$$

be the mean velocity fields (the distinction between mean and physical velocities arise only for the turbulent case). Let (x, y) be the length co-ordinates of a point with respect to the axes in Figure 1. We non-dimensionalize the variables as

$$\begin{gathered} x \equiv hx,\ y \equiv hy,\ \Delta(x) \equiv h\delta(x),\ u_I(x,y) \equiv Uu_I(x,y), \\ v_I(x,y) \equiv Uv_I(x,y),\ \mathcal{T}_I(x,y) \equiv (\Delta\mathcal{T})\,T_I(x,y), \\ p_I(x,y) \equiv \rho_I U^2 \pi_I(x,y) + p_o, \end{gathered} \tag{2}$$

where h is the gap between the plates, p_o is the inlet pressure, $\mathcal{T}_s(p_o)$ is the saturation temperature of the vapor at the inlet, $\mathcal{T}_{wo}$ is the uniform temperature of the bottom plate ($\mathcal{T}_{wo} < \mathcal{T}_s(p_o)$), $\Delta\mathcal{T} \equiv (\mathcal{T}_s(p_o) - \mathcal{T}_{wo})$ is the controlling temperature difference between the vapor and the plate, and U is the *average* inlet vapor speed determined by the inlet mass flux.

In the interior of either of the phases, the mass, momentum (x and y components), and the energy equation in differential forms are

$$\frac{\partial u_I}{\partial x} + \frac{\partial v_I}{\partial y} = 0, \tag{3}$$

$$u_I\frac{\partial u_I}{\partial x} + v_I\frac{\partial u_I}{\partial y} \approx -\frac{\partial \pi_I}{\partial x} + \frac{1}{Re_I}\frac{\partial(\sigma_I)_{xy}}{\partial y}, \tag{4}$$

$$0 \approx -\frac{\partial \pi_I}{\partial y}, \tag{5}$$

$$u_I\frac{\partial T_I}{\partial x} + v_I\frac{\partial T_I}{\partial y} \approx \frac{1}{Re_I Pr_I}\frac{\partial(q_I)_y}{\partial y}, \tag{6}$$

where

$$Re_I \equiv Uh/\nu_I,\ \nu_I \equiv \mu_I/\rho_I,\ \alpha_I \equiv k_I/(\rho_I C_{pI}),\ \text{and}\ Pr_I \equiv \nu_I/\alpha_I. \tag{7}$$

The non-dimensional values of shear stress $(\sigma_I)_{xy}$ and heat flux $(q_I)_y$ are related to the physical values of shear stress $(\tau_I)_{xy}$ and heat flux $(\mathcal{q}_I)_y$ by the relations

$$\begin{aligned} (\tau_I)_{xy} &\equiv (\mu_I U/h)\,(\sigma_I)_{xy}, \\ (\mathcal{q}_I)_y &\equiv (k_I \Delta\mathcal{T}/h)\,(q_I)_y. \end{aligned} \tag{8}$$

For laminar or turbulent flows of vapor, our method only needs the values of the vapor shear $(\tau_2)_{xy}$ at the interface ($y=\delta(x)$) and at the upper wall ($y=1$). For these stresses, shown in Figure 1, we define the friction factors f and f_u through the relations

$$\begin{aligned} \tau_f(x) &\equiv (\tau_2)_{xy}\big|_{y=\delta(x)} \equiv \frac{1}{2}\rho_2 (U u_{av}(x))^2 f\ , \\ \tau_w^u(x) &\equiv \left|(\tau_2)_{xy}\big|_{y=1}\right| \equiv \frac{1}{2}\rho_2 (U u_{av}(x))^2 f_u\ , \end{aligned} \tag{9}$$

where the non-dimensional average speed $u_{av}(x)$ of the vapor at any location x is given by

$$u_{av}(x) \equiv \frac{1}{1-\delta(x)} \int_{\delta(x)}^{1} u_2(x,y)\,dy\ . \tag{10}$$

The definition of U is

$$U \equiv \frac{1}{h}\int_0^h u_2(0,y)\,dy. \tag{11}$$

Therefore (10) and (11) imply

$$u_{av}(0) = 1\ . \tag{12}$$

■ The interface conditions, under very well established approximations ([3], [4]), simplify as listed below. The normal component of momentum balance, at the interface reduces to

$$\pi(x) \equiv \pi_2(x,\delta(x)) \cong \frac{\rho_1}{\rho_2}\pi_1(x,\delta(x)), \tag{13}$$

the tangential component of momentum balance at the interface (for laminar liquid and laminar or turbulent vapor) reduces to

$$\frac{\partial u_1}{\partial y}(x,\delta(x)) = \frac{1}{2}\frac{\mu_2}{\mu_1} Re_2 (u_2)_{av}^2 f, \tag{14}$$

the mass balance at the interface reduces to

$$\dot{m} \equiv \frac{\rho_2}{\rho_1}\left[u_2(x,\delta(x))\frac{d\delta}{dx} - v_2(x,\delta(x))\right]$$
$$= \left[u_1(x,\delta(x))\frac{d\delta}{dx} - v_1(x,\delta(x))\right], \tag{15}$$

the requirement of continuity of tangential component of velocities at the interface reduces to

$$u_1(x,\delta(x)) = u_2(x,\delta(x)) \equiv u_f(x), \tag{16}$$

the temperature at the interface is given by

$$T_1(x,\delta(x)) = T_2(x,\delta(x))$$
$$= \frac{1}{\Delta\mathcal{T}}\{\mathcal{T}_s(\rho_2 U^2 \pi(x) + p_o)\} \equiv T_s(\pi(x)), \tag{17}$$

and the energy equation at the interface is given by

$$\dot{m}(x) = \frac{Ja}{Re_1 Pr_1 \varphi_{fg}(x)}\left\{\frac{\partial T_1}{\partial y}(x,\delta(x)) - \frac{k_{2e}}{k_1}\frac{\partial T_2}{\partial y}(x,\delta(x))\right\}, \tag{18}$$

where k_{2e} is the effective thermal conductivity for laminar or turbulent vapor flow.

In (18) above, ϕ_{fg} is the ratio of jump in enthalpy (or heat of vaporization $\mathcal{h}_{fg}$) at any point on the interface to its value $\mathcal{h}^0_{fg}$ at the inlet. That is

$$\varphi_{fg}(\pi(x)) \equiv \frac{\mathcal{h}_{fg}(\pi(x))}{\mathcal{h}^0_{fg}}, \tag{19}$$

and Ja is

$$Ja \equiv \frac{C_{p1}\Delta\mathcal{T}}{\mathcal{h}^0_{fg}}. \tag{20}$$

- The wall conditions at y = 0 are

$$u_1(x,0) = v_1(x,0) = 0,$$
$$T_1(x,0) = T_w \equiv \mathcal{T}_{w0}/\Delta\mathcal{T}. \tag{21}$$

- The wall conditions at the upper wall (y = 1) are

$$u_1(x,1) = v_1(x,1) = 0, \tag{22}$$

and T_2 (x,1) = a prescribed constant above the non-dimensional saturation temperature at the inlet.

- In addition, the inlet conditions specifying pressure and average speed of the vapor, by virtue of their non-dimensional definitions in (2) and (10), are written as

$$u_{av}(0) = 1,$$
$$\pi_2(0,y) = 0. \tag{23}$$

- The onset of condensation at x = 0 is given by the requirement

$$\delta(0) = 0. \tag{24}$$

3. FURTHER APPROXIMATIONS FOR THIN FILM FLOWS

The lengths of duct, inlet Reynolds numbers, and temperature differences considered here correspond to thin films of the liquid condensate which move sluggishly. Simple scaling of the governing equations suggest that inertia of the condensate can be ignored provided $Re_1 u_f \delta^2 \ll 1$. Similarly convection in the film can be ignored compared to conduction provided $Re_1 Pr_1 u_f \delta^2 \ll 1$. However the above estimates for ignoring inertia and convection are *conservative* for flow of non-metallic vapors.This approximation is commonly used ([10], [2], etc.) for flow of non-metallic vapors and is justified over a larger range of flow parameters according to calculations of Koh [4]. He considered *laminar* forced film condensation flow over a horizontal flat plate while fully accounting for liquid inertia and convection. He showed that the effect of condensate inertia and convection was negligible for all speeds of non-metallic vapors, most temperature differences (say, $0 \le \Delta\mathcal{T} \le 60°C$), and commonly encountered liquid Prandtl numbers of $1 \le Pr_1 \le 10$. Under this approximation, then, equations (4) and (6) for liquid momentum and energy balance respectively reduce to

$$0 \cong -\frac{\partial \pi_1}{\partial x} + \frac{1}{Re_1}\frac{\partial^2 u_1}{\partial y^2}, \tag{25}$$

and

$$0 \cong \frac{1}{Re_1}\frac{\partial^2 T_1}{\partial y^2}. \tag{26}$$

Using the fact that (5) implies insignificant pressure variations in the transverse direction, we can write

$$\pi_2(x, y) = \pi_2(x, \delta(x)) \equiv \pi(x) \tag{27}$$

for all $\delta(x) \le y \le 1$, and

$$\pi_1(x, y) = \pi_1(x, \delta(x)) \equiv \pi_1(x) \tag{28}$$

for all $0 \le y \le \delta(x)$; and because of (13)

$$\pi(x) = \frac{\rho_1}{\rho_2}\pi_1(x). \tag{29}$$

Solving (25) for u_1 subject to (22), (14), (27)-(29), we find that the liquid condensate velocity profile is given as

$$u_1(x,y) = \frac{\mu_2}{\mu_1}Re_2\left[\left(-\frac{d\pi}{dx}\right)y\left(\delta(x) - \frac{y}{2}\right) + \frac{1}{2}u_{av}^2(x)\,fy\right]. \tag{30}$$

Solving (26) subject to (17) and (21) gives

$$T_1(x,y) = (T_s(\pi(x)) - T_w)\left(\frac{y}{\delta(x)}\right) + T_w\ . \tag{31}$$

Equation (18) can be rearranged to state that heat conducted from the film to the bottom wall is the sum of the latent heat released at the interface and the heat conducted by the vapor to the film. It is well known that even for superheated vapors ($0 \leq \Delta\mathcal{T}_{sup} \leq 15°C$), the value of latent heat released at the interface is significantly larger than any heat conducted from the vapor to the film. Scaling of (18) suggests that this is the case provided $(k_{2e}\Delta\mathcal{T}_{sup}/\ k_1\Delta\mathcal{T})\delta(x) << 1$. Under this common situation, (18) simplifies to

$$\dot{m}(x) \cong \frac{Ja}{Re_1 Pr_1 \varphi_{fg}(x)}\left[\frac{\partial T_1}{\partial y}(x,\delta(x))\right]\ . \tag{32}$$

In the light of (32), negligible contribution to heat transfer comes from vapor superheat, and hence one can ignore the vapor (I = 2) energy equation (6) because it is automatically satisfied under the approximation

$$T_2(x,y) \cong \text{an average constant.} \tag{33}$$

4. THE PROPOSED INTERGRAL - DIFFERENTIAL SCHEME AND ITS DIFFERENCES FROM THE USUAL APPROXIMATE TECHNIQUES

We intend to develop a reliable solution scheme for local variations in the lower dimensional unknowns (film thickness δ (x), heat transfer rates, etc.) which will allow for different admissible models for interfacial friction. This can be accomplished by satisfying the vapor momentum balances and mass balance in an integral sense (using the integrated forms of these laws) while satisfying *exactly* the remaining differential conditions (including the important interface conditions (13)-(18), equations (25)-(27) for the liquid condensate, etc.). However one should clearly understand the <u>difference</u> between the rationale of this approach and many integral approaches ([11], [13], [36], [43], etc.) which do not give accurate results. In some of the earlier works (as in [11]) for laminar flow of the vapor, the solution methodology found the interfacial shear $\tau_f(x)$ from the relation

$$\tau_f(x) = \mu_2\frac{\partial u_2}{\partial y}(x,\Delta(x)), \tag{34}$$

where $u_2(x, y)$ is an *assumed* vapor profile. In other works ([13], [36], etc.), a friction factor model

is *assumed* at the outset to solve the problem for film thickness δ (x), heat transfer rates, etc.

Our approach here is new because it consists of:

(a) not *assuming* a friction factor model, but *finding* a model which predicts the flow in accord with reliable experimental data, and

(b) showing that for any *given* model of interfacial friction factor f, the solution of the lower dimensional unknowns (film thickness $\delta(x)$, average vapor speed u_{av} (x), etc.) are insignificantly affected by the choice of vapor velocity profile u_2 (x,y) over $\delta(x) \leq y \leq 1$.

The integrated form of vapor mass balance simply states that the sum of vapor mass flux and liquid mass flux at any x is a constant for steady flows, and is given by

$$\frac{\rho_2}{\rho_1}\int_{\delta(x)}^{1} u_2(x,y)\,dy + \int_{0}^{\delta(x)} u_1(x,y)\,dy = \frac{\rho_2}{\rho_1}. \tag{35}$$

Equation (35) above also follows from integrating the continuity equations in (3) for I = 1 and 2 and inserting the resulting expressions in the interface mass balance (15).

The integrated form of vapor momentum balance simply states that, at any location x, the algebraic sum of pressure force, frictional force, and "kick-back" force (associated with interface mass transfer) per unit length equals the cross-sectional rate of change of momentum-flux. This is given as

$$-\frac{d\pi}{dx}(1-\delta(x)) - \frac{1}{2}u_{av}^2(x)\,(f+f_u) - \frac{\rho_1}{\rho_2}\dot{m}(x)\,u_f(x) = \frac{d}{dx}\left[\int_{\delta(x)}^{1} u_2^2(x,y)\,dy\right], \tag{36}$$

where equation (36) above is an integrated form of (4) over $\delta(x) \leq y \leq 1$. One can derive (36) by combining equations (35), (9), (16), and (27) with an integral of (4) for I = 2.

If we satisfy the interface energy equation (32), total mass balance (35), and vapor momentum balance (36) for liquid velocity and temperature profiles respectively given by (30) and (31), then we would have satisfied *all* the *differential* downstream evolution equations of section 3 (which are *elliptic* in the transverse direction and *parabolic* in the downstream direction).

The proposed method consists of the following steps:

(i) Make a choice for vapor velocity profile; for example, consider uniform vapor velocity profile

$$u_2(x,y) = u_{av}(x) \tag{37}$$

for $\delta(x) \leq y \leq 1$, or, consider $u_2(x,y)$ to be *close* to a turbulent vapor velocity profile (see [44], p. 460), satisfying the speed restrictions in (16) and (22), given as

$$u_2(x,y) = U_0(x)\,[1 - a\eta^2 - (1-a)\,\eta^{2m}] + u_f(x)\left[\frac{1-y}{1-\delta(x)}\right], \tag{38}$$

where

$$\eta = 2\left(\frac{y-\delta(x)}{1-\delta(x)}\right) - 1, \qquad a = 0.354, \qquad 2m = 32, \tag{39}$$

U_0 (x) is to be determined, and interface speed u_f (x) is obtained by setting y = δ (x) in (30). A *typical* computed profile utilizing (38) is shown in Figure 2.

(ii) Solve the problem (equations (32), (35), and (36)) for either of the choices ((37) or (38)) and show, as in Figure 3, that the solution is nearly independent of the choice of vapor velocity profile for any *given* friction factor model. This establishes the soundness of this approach.

(iii) For any one choice of vapor velocity profile, find a friction factor model for f which yields results in agreement with reliable experimental data.

Having stated the steps and shown the results in Figure 3, for brevity, we *only* outline here the methodology for the choice in (37). The formulation for the profile in (38) can be similarly obtained.

Equation (32) with $\dot{m}$ given by $\frac{\rho_2}{\rho_1}\frac{d}{dx}\left(\int_\delta^1 -u_2 dy\right)$ —an integral form of (15), and equations (35) and (36) are the governing equations. Substituting (30), (31), and (37) in them, we can respectively write these three equations as

$$\mathbf{A}(\mathbf{y})\frac{d\mathbf{y}}{dx} = \mathbf{b}(\mathbf{y}, f, f_u) \tag{40}$$

where

$$\mathbf{A} \equiv \begin{bmatrix} 1 & 0 & 0 \\ 0 & A_{22}(\mathbf{y}) & A_{23}(\mathbf{y}) \\ 0 & A_{32}(\mathbf{y}) & A_{33}(\mathbf{y}) \end{bmatrix}, \qquad \mathbf{b}(\mathbf{y}) \equiv \begin{bmatrix} b_1(\mathbf{y}, f) \\ b_2(\mathbf{y}) \\ b_3(\mathbf{y}, f, f_u) \end{bmatrix},$$

$\mathbf{y} \equiv [\pi(x), u_{av}(x), \delta(x)]^T$ and the scalar functions A_{22}, A_{23}, A_{32}, A_{33}, b_1, b_2, and b_3 are defined in equations (A.1) to (A.10) of the Appendix. The interfacial friction factor f is to be *determined*. The upper wall, which is dry, has a friction factor f_u (see definition in (9)) and can be *estimated* because it is a nearly parallel single phase flow at the upper wall. Because of the dominance of interfacial friction f in driving the condensate, it turns out that the predictions of the flow variable is not sensitive to the *estimate* on f_u. For two different inlet conditions, we make two different estimates on f_u. If the vapor flow is assumed to be fully developed and turbulent prior to the inlet, the shear can be assumed to remain close to the fully developed turbulent values at the upper wall. This means, using a friction factor for fully developed turbulent flow between parallel

plates (see p. 487, in [44]), we can estimate

$$f_u \cong 0.0713\,(Re_2 u_{av}(x))^{-0.25} \equiv f_0. \tag{41}$$

Alternatively if a shear free vapor enters as a uniform flow, we expect a laminar and subsequently turbulent boundary layers over the upper plate. If this was to happen, for flow conditions (see (67) below) investigated in this paper, the boundary layers continue to *develop* over $0 \le x \le 40$. For this situation, we estimate (see [33]) f_u as

$$f_u \cong 0.664\,(Re_2 u_{av}(x)\,x)^{-0.5} \quad \text{for} \quad Re_2 u_{av}(x)\,x \le 5 \times 10^5, \tag{42}$$

and

$$f_u \cong 0.0592\,(Re_2 u_{av}(x)\,x)^{-0.2} \quad \text{for} \quad Re_2 u_{av}(x)\,x \ge 5 \times 10^5. \tag{43}$$

The result in Figure 4 confirms that for any chosen f, the estimate on f_u, whether by (41) or (42)-(43), has an *insignificant* higher order effect on the significant flow variables. Hence an *accurate* estimate of f_u is a *non-issue*. In what follows, unless otherwise stated, f_u is given by (41).

5. FUNDAMENTAL NEW RESULTS ON INTERFACIAL FRICTION FACTOR f AND A MATHEMATICAL THEOREM FOR THE SOLUTION OF THE PROBLEM

An inspection of the non-dimensional parameters appearing in (40) yields the fact that we have a minimal set of four independent non-dimensional parameters:

$$\{Re_{in}, \frac{Ja}{Pr_1}, \frac{\rho_2}{\rho_1}, \frac{\mu_2}{\mu_1}\}. \tag{44}$$

Here $Re_{in} \equiv Re_2$ and Ja/Pr_1 are respectively viewed as non-dimensional *control* parameters of inlet speed U and temperature difference $\Delta\mathcal{T}$. The density ratio ρ_2/ρ_1 and viscosity ratio μ_2/μ_1 are viewed as *passive* fluid parameters. In fact when the interface is *wavy*, one must include any additional non-dimensional parameters that appear in the equations governing the evolution of superposed disturbances. This means that there is an additional *gravity parameter* $U/\sqrt{gh}$, the Froude number, that should be added to the set in (44). However for the geometry under consideration, if the gap width h is large (say greater than ten times the film thickness at all locations) and g is constant (this excludes microgravity environment) then this parameter's influence is entirely accounted for by the Reynolds number Re_{in}. Since this paper stays within the constraints of fixed g and large h, in what follows, we would not explicitly show the presence of Froude number in the set specified in (44). The problem of solving (40) over $x \ge 0$ subject to the initial conditions (23)-(24) is equivalently posed as

$$\frac{dy}{dx} = A^{-1}b \equiv g(y, f),$$
$$f = f\left(x, Re_{in}, \frac{Ja}{Pr_1}, \frac{\rho_2}{\rho_1}, \frac{\mu_2}{\mu_1}\right), \tag{45}$$
$$y(0) = [0, 1, 0]^T,$$

where $y \equiv [\pi(x), u_{av}(x), \delta(x)]^T$, $g \equiv [g_1, g_2, g_3]^T$ and components g_1, g_2, and g_3 of **g** are defined in equations (A.1) - (A.13) of the Appendix A. Note that the friction factor f in (45), like any of the flow variables in **y**, can, *at most*, depend on the distance x and the non-dimensional parameters listed in (44). The issue now is our ability to solve (45) for *any* friction factor f in $(45)_2$. If (45) was a *well posed initial value problem* (see, e.g., p. 400 of [45]), then the system of ordinary differential equations can always be solved numerically for any f. However, the function **g** in (45) has singularities for $x \sim 0$ because of the requirement $\delta(0) = 0$. Despite this, (45) may be integrable, much in the same way as the equation $d\delta(x)/dx = 1/\delta(x)$ subject to $\delta(0) = 0$ is integrable and has a solution $\sqrt{2x}$.

An inspection of the function **g**, in combination with verification by computer algebra, proves the following theorem:

THEOREM: There exists a solution of (45) satisfying the initial condition $(45)_3$ if any only if the friction factor is of the form

$$f = 8\left(\frac{Ja}{Pr_1}\right)\left(\frac{\rho_2}{\rho_1}\right)\left(\frac{\mu_2}{\mu_1}\right)^{-2}(Re_{in})^{-2}\frac{1}{c_1^3}\frac{1}{x^{1/2}} + O(1) \tag{46}$$
$$= \left(8Re_{in}\frac{\mu_1}{\mu_2}\right)\frac{1}{c_1^2}\dot{m}(x) + O(1) \quad ,$$

where the constant c_1 is the zero of a well defined non-linear function ψ (see proof below for definition) and satisfies an equation of the form

$$\psi\left(c_1, Re_{in}, \frac{Ja}{Pr_1}, \frac{\rho_2}{\rho_1}, \frac{\mu_2}{\mu_1}\right) = 0. \tag{47}$$

Furthermore for f as in (46), the solution of (45), over a small neighborhood $0 \le x \le \varepsilon$, is of the form

$$y(x) = y_0 + y_1 x^{1/2} + y_2 x + y_3 x^{3/2} + o(x^{3/2}), \tag{48}$$

where $y_0 = y(0) = [0, 1, 0]^T$, $y_1 \equiv [c_3, -c_2, c_1]^T$, $y_2 \equiv [\hat{k}_1, \hat{c}_2, \hat{c}_1]^T$, and $y_3 \equiv [\bar{k}_1, \bar{c}_2, \bar{c}_1]^T$, are

constant vectors.

Proof Outline:

■ (⇒)

If we assume f is of the form given by (46), then it can be shown that there exists a solution of the type given by (48). To show this, substitute (46) and (48) in the function **g**(**y**,f) on the right side of (45). On asymptotic expansion of **g** using symbolic mathematics on the computer, we find

$$\mathbf{g}(\mathbf{y}, f) = \mathbf{d}_1 x^{-1/2} + \mathbf{d}_2 + \mathbf{d}_3 x + o(x^{1/2}), \tag{49}$$

where the constant vectors $\mathbf{d}_1$, $\mathbf{d}_2$, $\mathbf{d}_3$, etc. are easily obtained from computer algebra. Substituting the three term expansions in (48) and (49) in (45), and matching coefficients of x, we find that

$$\begin{aligned} \mathbf{y}_1/2 &= \mathbf{d}_1(\mathbf{y}_1, \mathbf{y}_2, \mathbf{y}_3), \\ \mathbf{y}_2 &= \mathbf{d}_2(\mathbf{y}_1, \mathbf{y}_2, \mathbf{y}_3), \\ 3\mathbf{y}_3/2 &= \mathbf{d}_3(\mathbf{y}_1, \mathbf{y}_2, \mathbf{y}_3). \end{aligned} \tag{50}$$

It can be verified that the number of equations obtained by matching coefficients of x , as in (50) above, is always equal to the number of unknowns regardless of the number of terms used in the expansions of (48) and (49). Furthermore, the equations obtained by matching the coefficients of x, such as (50), have the simplifying feature that they are <u>linear</u> in the vectors $\mathbf{y}_2$, $\mathbf{y}_3$, etc. but non-linear in the vector $\mathbf{y}_1$. An analytical proof of the convergence of the asymptotic solution (48) to the real solution is not offered here. However we show numerically, by means of a sample calculation shown in Table 2, the convergence of the vector $\mathbf{y}_1$ *and* therefore of the asymptotic solution to the actual solution at small x. We found that in all cases, a three term expansion in (48) was adequate to allow a numerical solution beyond $x \geq \varepsilon > 0$ for some small ε. This was always possible, perhaps because, in the neighborhood of **y**(ε) (but <u>not</u> **y**(0)), all the Lyapunov exponents (see [46]) are negative and the numerical solution rapidly converge and come arbitrarily close to the *attracting* solution beyond $x \geq 0.2$.

For the three term expansion, manipulation of the nine scalar equations in (50) gives

$$\begin{aligned} c_2 &= c_2(c_1), \\ \hat{c}_1 &= \hat{c}_1(c_1, c_2), \\ \hat{c}_2 &= \hat{c}_2(c_1, c_2, \hat{c}_1), \\ \bar{c}_1 &= \bar{c}_1(c_1, c_2, \hat{c}_1, \hat{c}_2), \text{ and} \\ \bar{c}_2 &= \bar{c}_2(c_1, c_2, \hat{c}_1, \hat{c}_2, \bar{c}_1). \end{aligned} \tag{51}$$

Therefore if c_1 is known, the constants on the left side of the five equations in (51) can be sequentially calculated with the help of the right side functions defined in (B.1)-(B.13) of Appendix B. The constants $k_1, \hat{k}_1, \text{and}\, \bar{k}_1$ can then be calculated with the help of three of the remaining equations implied by (50) and given as (B.15)-(B.17) in Appendix B. The constant c_1 itself has to satisfy the only remaining equation in (50), namely $\psi = 0$ (see (47)), where ψ is

defined in (B.18)-(B.20) of Appendix B.

The above procedure can be extended to an n term expansion ($n \geq 3$) to find the limiting and convergent form of ψ as $n \rightarrow \infty$. From this limiting form one then finds the convergent value of c_1 and vector $\mathbf{y}_1$.

For application purposes, the <u>admissible</u> zero of ψ (for which one obtains a convergent solution of the type presented in Table 2) can be estimated over a specified parameter range (given by (67) below) by the correlation

$$= 0.60135\left(\frac{\rho_2}{\rho_1}\right)^{-0.3455}\left(\frac{\mu_2}{\mu_1}\right)^{-0.0020}\left(\frac{Ja}{Pr_1}\right)^{0.3226} Re_{in}^{-0.407} \tag{52}$$

The acceptable accuracy level of the correlation in (52) can be seen in Table 3.

■ ($\Leftarrow$)

The three component equations of (45), written in terms of the three components of the original equation (40), are given by

$$\frac{d\pi}{dx} = -\frac{3}{\delta^3(x)}\left[\frac{\mu_1}{\mu_2}\frac{1}{Re_2}\frac{\rho_2}{\rho_1}\{1-u_{av}(x)\,(1-\delta(x))\} - \frac{1}{4}u^2_{av}(x)\,f\delta^2(x)\right], \tag{53}$$

$$\{-\frac{\rho_2}{\rho_1}(1-\delta(x))\,\delta(x)\}\frac{du_{av}}{dx} + \{\frac{\rho_2}{\rho_1}u_{av}(x))\,\delta(x)\}\frac{d}{dx}\delta(x) = \frac{Ja}{Pr_1}\frac{1}{Re_1}\frac{[T_s(\pi(x)) - T_w]}{\varphi_{fg}(\pi(x))}, \text{ and} \tag{54}$$

$$\{2(1-\delta(x))\,u_{av}(x)\}\frac{du_{av}}{dx} + \{-u^2_{av}(x)\}\frac{d}{dx}\delta(x) = -\frac{d\pi}{dx}(1-\delta(x)) - \frac{1}{2}u^2_{av}(x)\,(f+f_u) - \frac{\rho_1}{\rho_2}\dot{m}u_f, \tag{55}$$

where $\dot{m}$ and u_f are as defined in (A.9) and (A.10) of Appendix A. From the definitions (17), (19), and (21) it follows that (A.9) implies

$$\lim_{x\to 0}(\dot{m}\delta) = \lim_{x\to 0}\left(\frac{Ja}{Pr_1}\frac{1}{Re_1}\frac{[T_s(\pi(x)) - T_w]}{\varphi_{fg}(\pi(x))}\right) = \frac{Ja}{Pr_1}\frac{1}{Re_1} \equiv B_1, \tag{56}$$

where B_1 is a constant. Furthermore, under

$$\pi(0) = 0, \qquad u_{av}(0) = 1, \quad \text{and} \qquad \delta(0) = 0 \tag{57}$$

we find that as $x \rightarrow 0$, the left and right sides of (54) yield

$$-\frac{\rho_2}{\rho_1}\lim_{x\to 0}\left(\delta(x)\frac{du_{av}}{dx}\right) + \frac{\rho_2}{\rho_1}\lim_{x\to 0}(\delta(x)\frac{d\delta}{dx}) \equiv B_1. \tag{58}$$

In writing (58) we have assumed that $\delta(x)$ and $u_{av}(x)$ are such that the limit of the sum of the terms on the left side of (54) equals the sum of the limits as

$$\lim_{x\to 0}\left(\delta(x)\frac{du_{av}}{dx}\right) \equiv \frac{c_1^2}{2} \quad \text{and}$$
$$\lim_{x\to 0}(\delta(x)\frac{d\delta}{dx}) \equiv -\frac{c_1 c_2}{2} \tag{59}$$

exist. It follows that

$$\delta(x) = c_1 x^{1/2} + o(x^{1/2}), \text{ and}$$
$$u_{av}(x) = 1 - c_2 x^{1/2} + o(x^{1/2}). \tag{60}$$

Equation (58) then implies

$$c_2 = 2\frac{B_1}{c_1}\frac{\rho_1}{\rho_2} - c_1. \tag{61}$$

From physical considerations, we require that the total pressure force per unit length on the liquid condensate $(0 \le y \le \delta(x))$ be *finite* at all $x \ge 0$. This force is found to be proportional to $(d\pi/dx)\,\delta(x)$, it then follows that we require

$$\lim_{x \to 0} \{\frac{d\pi}{dx}\delta(x)\} = \text{some finite number}. \tag{62}$$

Equation (57) and (62) together imply that there is a constant k_1 such that

$$\pi(x) = k_1 x^{1/2} + o(x^{1/2}). \tag{63}$$

Substituting for $d\pi/dx$ from (53) in (62), we find that

$$\lim_{x \to 0}\left[4\frac{\rho_2}{\rho_1}\frac{\mu_1}{\mu_2}\frac{1}{Re_2}\{\frac{1-u_{av}(x)\,(1-\delta(x))}{(\delta(x))^2(u_{av}(x))^2}\} - f\right] \tag{64}$$

must be finite. Substitution of (60) and (61) in (64) then implies that finite limit is possible only if f is as given by $(46)_1$. With f as in $(46)_1$, it can be verified that the limiting form, as $x \to 0$, of (55) is consistent as each term behaves like $1/\delta(x)$.

If the original assumption that each of the limits in (59) existed was not correct then the limiting form of the left side of (54) may still be meaningful provided the limit of the two terms taken together exists. If this was to be the case, it can be shown that it is impossible to find an f (x) for x~0 which will lead to self consistent limiting forms of (53) and (55) while meeting the requirement in (62). This fact is verified by seeking δ (x), $\{1-u_{av}(x)\}$, and f (x) in the form $x^{\alpha 1}$, $x^{\alpha 2}$, and $x^{\alpha 3}$ and then showing the impossibility of finding $\alpha 1$, $\alpha 2$, and $\alpha 3$ which lead to all equations being satisfied consistently at x~0.

The above arguments established that for x~0, f is of the form given by (46) and that the solution is of the form given by (48).

End of Proof Outline

The result in (46) is easily interpreted. At the onset of condensation (x ~ 0), the vapor suction rate $\dot{m}$ (given by (A.9) in the Appendix) is very high, so the suction effect dominates and determines the friction factor as

$$f \sim f_{asy} \equiv \left(8Re_{in}\frac{\mu_1}{\mu_2}\right)\frac{1}{c_1^2}\dot{m}. \tag{65}$$

Based on this expectation of dominance of the suction effect, Shekriladze and Gomelauri

[5], and subsequently Linehan, et al. [47], and Jensen and Yuen [48] proposed their models. However they based the form of their formulas on an adaptation of a classical solution (p. 368, [33]) of Navier-Stokes equations for flow over a flat plate with suction. Their model and the result in (65) above agree with regard to proportionality to $\dot{m}$, but the proportionality constant differs. The proportionality constant here is determined from first principles and this is vital for developing a working algorithm for a solution of (45). In fact, all of the commonly used models ([5], [23], [37], etc.) cannot satisfy the initial conditions $(45)_3$ and solutions are commonly obtained by a tedious trial and error selection of non-zero values of π, u_{av}, and δ at some small value of x.

The value of an explicit $f \sim f_{asy}$ for $x \sim 0$ lies mainly in the fact that it provides a *working tool* for solution of (45) for a general f of the form given in (45), or equivalently, of the form

$$f = \begin{cases} f_{asy} & \text{for } x \le \varepsilon \\ f_{reg}(x, Re_{in}, Ja/Pr_1, \rho_2/\rho_1, \mu_2/\mu_1) & \text{for } x \ge \varepsilon. \end{cases} \tag{66}$$

In (66) above, the value of f_{reg} equals the value of f_{asy} at an $x = \varepsilon$ (Re_{in}, Ja/Pr_1, ρ_2/ρ_1, μ_2/μ_1). Since f_{asy} drops rapidly from $+\infty$ to a finite positive value (see Figure 6), many of the commonly used models can be tested as f_{reg} in (66) if an appropriate choice of ε is made. This is done and the results are shown in Figure 5.

6. ROLE AND AVAILABILITY OF RELIABLE EXPERIMENTAL DATA

If one has a correct estimate of friction factor f, then the film thickness variations δ (x), or its manifestation, the heat transfer to the bottom plate in Figure 1, should be in accord with experimental measurements. This is because the governing equations (45), except for a model for f, are well established.

Therefore reliable and accurate experimental data is vital. The data of Lu [15] is reliable because his estimates on heat transfer rates have been consistently obtained by two to three different and independent measurement approaches. For example, heat transfer rates were measured by (a) an energy balance on the coolant flowing under the bottom plate of Figure 1, (b) an overall energy balance for the flow in the duct in combination with experimentally measured values of total mass flux at the inlet and the mass flux of the liquid condensate at the outlet ($x \cong 40$), and (c) an estimate on heat transfer rates from experimentally measured (only for flow regimes involving smooth interface) values of film thickness variations. Based on the current availability of data [15] for flow of R-113 (Freon family) and FC-72 (Fluorinert Carbon) vapor, we consider the parameter set (44) in the restricted range

$$
\begin{aligned}
0 \le x \le 40, \\
0.004 \le \rho_2/\rho_1 \le 0.009, \\
0.016 \le \mu_2/\mu_1 \le 0.026, \\
0.009 \le Ja/Pr_1 \le 0.045, \\
9,500 \le Re_{in} \le 90,000.
\end{aligned}
\tag{67}
$$

Since the *actual* variations in density and viscosity ratios in each of the two fluids is *limited*, in reality we do not have much independent variation capability of these two ratios. In fact we can treat the available data as:

$$
\begin{aligned}
\frac{\rho_2}{\rho_1} \cong \left(\frac{\rho_2}{\rho_1}\right)_{av} &= \begin{cases} 0.0050 & \text{for} \quad R-113 \\ 0.0082 & \text{for} \quad FC-72 \end{cases} \\
\frac{\mu_2}{\mu_1} \cong \left(\frac{\mu_2}{\mu_1}\right)_{av} &= \begin{cases} 0.0185 & \text{for} \quad R-113 \\ 0.0218 & \text{for} \quad FC-72 \end{cases}
\end{aligned}
\tag{68}
$$

In addition to heat transfer rates, Lu's experiments [15] also provide an estimate on an inlet Reynolds number Re_L up to which ($Re_{in} \le Re_L$ (Ja/Pr_1, ρ_2/ρ_1, μ_2/μ_1)) the interface is smooth and an estimate on inlet Reynolds number Re_U above which ($Re_{in} \ge Re_U$ (Ja/Pr_1, ρ_2/ρ_1, μ_2/μ_1)) the interface is fully rough with steady three dimensional wave patterns over the entire interface. Experimental data (see Tables 6.3 and 6.4 of [15]) in the parameter range given by (67), noting the restriction on x, provide an estimate on Re_L and Re_U described above. The estimates are:

$$
\begin{aligned}
Re_L &\cong a_1(\rho_2/\rho_1, \mu_2/\mu_1)\left(\frac{Ja}{Pr_1}\right)^{-0.2288}, \\
Re_U &\cong \hat{a}_1(\rho_2/\rho_1, \mu_2/\mu_1)\left(\frac{Ja}{Pr_1}\right)^{-0.2657},
\end{aligned}
\tag{69}
$$

where for density and viscosity ratios, as given in (68), a_1 and $\hat{a}_1$ are given in Table 4.

There is currently insufficient data for a *reliable* correlation with respect to density and viscosity ratios. However, if $(\mu_2/\mu_1)_{av}$ is considered approximately equal for both cases in (68), then (70), in the *limited* parameter range of (68), can be *tentatively* correlated as

$$
\begin{aligned}
a_1(\rho_2/\rho_1, \mu_2/\mu_1) &\cong a_{10}(\mu_2/\mu_1)(\rho_2/\rho_1)^{0.449}, \\
\hat{a}_1(\rho_2/\rho_1, \mu_2/\mu_1) &\cong \hat{a}_{10}(\mu_2/\mu_1)(\rho_2/\rho_1)^{0.824},
\end{aligned}
\tag{70}
$$

where a_{10} and $\hat{a}_{10}$ are given in Table 4.

7. THE PROPOSED MODEL FOR FRICTION FACTOR

A model of f is sought in any form which is equivalent to $(45)_2$ *and* belongs to the "admissible class" specified by (46). In fact, two models of f, which lead to predictions in agreement with experiments, may *appear* to be different but if their *values* are close for the same values of the arguments (i.e. x, Re_2, Ja/Pr_1, ρ_2/ρ_1, μ_2/μ_1) over a specified domain (as in (67)), then both are "good" models over that domain.

Before proposing a new model for f, we tested, for a typical flow situation, some of the common models for f as f_{reg} in (66) and the results are show in Figure 5. The common models did *poorly* with regard to quantitative predictions for both heat transfer rates and film thickness variations. However $f = f_{reg} = \beta f_0$, $\beta \cong 5.7$, as shown in Figure 5, did very well for the flow situation specified by case # 9 in Table 1. This suggests that one may seek a model for f_{reg} in its equivalent form

$$\begin{aligned} f_{reg} &= f\left(x, Re_{in}, \frac{Ja}{Pr_1}, \frac{\rho_2}{\rho_1}, \frac{\mu_2}{\mu_1}\right) \\ &= \beta f_0(x), \end{aligned} \tag{71}$$

where $\beta = \beta\ (Re_{in}, Ja/Pr_1, \rho_2/\rho_1, \mu_2/\mu_1)$ and f_0 is the friction factor given in (41) as f_u. Our approach then is to solve (45) with f as in (53) and (59) and find β such that the overall heat transfer rates over $0 \le x \le 0.899$ m is the same for the theory and the experiment ([15]). We set, for the flow in Figure 1, gap h = 0.025 m and plate width w = 0.04 m to model the rectangular cross-section of the experiment. For brevity, we only show some sample values of β in column 7 of Table 5. These sample values of β were found by requiring good agreement between the model and experimental predictions with regard to overall heat transfer rates over $0 \le x \le 40$. The correlation for β is then found and the predictive capacity of the model is tested against several additional experimental runs (see rows in Table 5 for which β(run) is not listed) for both heat transfer rates and film thickness variations. The results of these comparisons are given in Table 5. It suffices here to note that the interfacial shear in (9) over the parameter range (67), is given by an f in the form

$$f = \begin{cases} f_{asy} & \text{for} \quad x \le \varepsilon \\ f_{model} & \text{for} \quad x \ge \varepsilon \end{cases} \tag{72}$$

where (combining $(46)_1$, (52), and the result $\delta(x) \cong c_1\sqrt{x}$ from (48) for a form of f_{asy})

$$f_{asy} = 22.15\left(\frac{\rho_2}{\rho_1}\right)^{1.69}\left(\frac{\mu_2}{\mu_1}\right)^{-1.996}\left(\frac{Ja}{Pr_1}\right)^{0.346} Re_{in}^{-1.186}\frac{1}{\delta(x)}, \tag{73}$$

$$f_{model} = \beta f_0, \qquad f_0 = 0.0713\,(Re_{in}u_{av}(x))^{-0.25}, \tag{74}$$

$$\beta = \begin{cases} \beta_0\left(Re_{in}, \frac{Ja}{Pr_1}, \frac{\rho_2}{\rho_1}, \frac{\mu_2}{\mu_1}\right) & \text{for} \quad Re_{in} \le Re_L \\ \beta_1\left(Re_{in}, \frac{Ja}{Pr_1}, \frac{\rho_2}{\rho_1}, \frac{\mu_2}{\mu_1}\right) & \text{for} \quad Re_{in} \ge Re_U, \end{cases} \tag{75}$$

and Re_L and Re_U are as defined in (69) - (70). The multiplier β_0 for *smooth* interface can be estimated from

$$\beta_0 = \begin{cases} (\beta_{00}) \left(\frac{Ja}{Pr_1}\right)^{1.6984} Re_{in}^{-1.4838} & \text{for} \quad Ja_1 \le \frac{Ja}{Pr_1} \le 0.045 \\ (\beta_{01}) \left(\frac{Ja}{Pr_1}\right)^{0.4485} Re_{in}^{-1.4838} & \text{for} \quad 0.009 \le \frac{Ja}{Pr_1} < Ja_1, \end{cases} \tag{76}$$

where the numbers $\beta_{00} = \beta_{00}\,(\rho_2/\rho_1, \mu_2/\mu_1)$ and $\beta_{01} = \beta_{01}\,(\rho_2/\rho_1, \mu_2/\mu_1)$ and Ja_1 in (76) are given in Table 4.

The multiplier β_1 for *wavy* interface can be estimated from

$$\beta_1 = \begin{cases} (\beta_{10}) \left(\frac{Ja}{Pr_1}\right)^{1.6816} Re_{in}^{2.034} & \text{for} \quad 0.024 \le \frac{Ja}{Pr_1} \le 0.045 \\ (\beta_{11}) \left(\frac{Ja}{Pr_1}\right)^{1.062} Re_{in}^{1.3689} & \text{for} \quad 0.009 \le \frac{Ja}{Pr_1} < 0.024, \end{cases} \tag{77}$$

where the numbers $\beta_{10} = \beta_{10}\,(\rho_2/\rho_1, \mu_2/\mu_1)$ and $\beta_{11} = \beta_{11}\,(\rho_2/\rho_1, \mu_2/\mu_1)$ in (77) are given in Table 4

Note that, in general,

$$\varepsilon = \varepsilon\,(Re_{in}, Ja/Pr_1, \rho_2/\rho_1, \mu_2/\mu_1)\,. \tag{78}$$

A correlation for ε can be given as

$$\varepsilon = \begin{cases} \varepsilon_0\left(Re_{in}, \frac{Ja}{Pr_1}, \frac{\rho_2}{\rho_1}, \frac{\mu_2}{\mu_1}\right) & \text{for} \quad Re_{in} \le Re_L \\ \varepsilon_1\left(Re_{in}, \frac{Ja}{Pr_1}, \frac{\rho_2}{\rho_1}, \frac{\mu_2}{\mu_1}\right) & \text{for} \quad Re_{in} \ge Re_U, \end{cases} \tag{79}$$

where

$$\varepsilon_0 = \begin{cases} (\varepsilon_{00}) \left(\frac{Ja}{Pr_1}\right)^{-3.3086} Re_{in}^{2.1118} & \text{for} \quad 0.025 \le \frac{Ja}{Pr_1} \le 0.045 \\ (\varepsilon_{01}) \left(\frac{Ja}{Pr_1}\right)^{-0.6515} Re_{in}^{2.1118} & \text{for} \quad 0.009 \le \frac{Ja}{Pr_1} < 0.025, \end{cases} \tag{80}$$

and

$$\varepsilon_1 = (\varepsilon_{10}) \left(\frac{Ja}{Pr_1}\right)^{-2.7904} Re_{in}^{-4.7206} \quad \text{for} \quad 0.009 \le \frac{Ja}{Pr_1} \le 0.045, \tag{81}$$

and ε_{00}, ε_{01}, and ε_{10} are given in Table 4. Here we note that typically ε lies within the range $10^{-5} \le \varepsilon \le 10^{-2}$ for the entire parameter range in (67). Its correlation is not significant because the solution away from x is not affected by the accuracy in the value of ε. In fact f_{asy} and f_{model} can also be matched as in (A.14)-(A.15) of the Appendix without any loss of accuracy in the solution for $x \ge 0.2$.

Although the correlations above are more useful as a predictive tool, a qualitative trend of the friction factor's variations with distance is shown, for two representative flow situations, in Figure 6. A direct correlation for f_{reg} in $(71)_1$ can also be given in the form

$$f_{reg} = \begin{cases} f_0\left(x, Re_{in}, \frac{Ja}{Pr_1}, \frac{\rho_2}{\rho_1}, \frac{\mu_2}{\mu_1}\right) & \text{for} \quad Re_{in} \le Re_L \\ f_1\left(x, Re_{in}, \frac{Ja}{Pr_1}, \frac{\rho_2}{\rho_1}, \frac{\mu_2}{\mu_1}\right) & \text{for} \quad Re_{in} \ge Re_U, \end{cases} \tag{82}$$

where

$$f_0 \cong \begin{cases} (f_{00}) \left(\frac{Ja}{Pr_1}\right)^{1.707} Re_{in}^{-1.8447} x^{0.0062} & \text{for} \quad 0.024 \le \frac{Ja}{Pr_1} \le 0.045 \\ (f_{01}) \left(\frac{Ja}{Pr_1}\right)^{0.362} Re_{in}^{-1.8447} x^{0.0062} & \text{for} \quad 0.009 \le \frac{Ja}{Pr_1} < 0.024, \end{cases} \tag{83}$$

and

$$f_1 \cong (f_{10}) \left(\frac{Ja}{Pr_1}\right)^{1.4447} Re_{in}^{1.611} x^{0.00388} \quad \text{for} \quad 0.009 \le \frac{Ja}{Pr_1} \le 0.045, \tag{84}$$

and the constants f_{00}, f_{01}, and f_{10} are given in Table 4.

Also note that the correlations given above and in the following section are improved versions of what was reported in Narain [12].

8. CORRELATIONS FOR FILM THICKNESS, HEAT TRANSFER RATES, PRESSURE DROPS, AND AVERAGE VAPOR SPEEDS

Since film thickness and heat transfer rate variations are of general use, besides their limited trend indicated in Figure 8, we present their approximate correlations (average error within ±15%) based on results over the parameter range (67). For film thickness, we write.

$$\delta = \begin{cases} \delta_0\left(x, Re_{in}, \frac{Ja}{Pr_1}, \frac{\rho_2}{\rho_1}, \frac{\mu_2}{\mu_1}\right) & \text{for} \quad Re_{in} \le Re_L \\ \delta_1\left(x, Re_{in}, \frac{Ja}{Pr_1}, \frac{\rho_2}{\rho_1}, \frac{\mu_2}{\mu_1}\right) & \text{for} \quad Re_{in} \ge Re_U, \end{cases} \tag{85}$$

where δ_0 is the thickness for smooth interface, and δ_1 is the *mean* thickness for wavy interface. The Reynolds numbers Re_L and Re_U are as specified in (69)-(70). The correlation for δ_0, over $x \ge 0.01$, is

$$\delta_0 = \delta_{00}(\rho_2/\rho_1, \mu_2/\mu_1)\left(\frac{Ja}{Pr_1}\right)^{0.2604} Re_{in}^{-0.2023} x^{0.3393}, \tag{86}$$

and the correlation for δ_1, over $x \ge 0.01$, is

$$\delta_1 = \delta_{10}(\rho_2/\rho_1, \mu_2/\mu_1)\left(\frac{Ja}{Pr_1}\right)^{\sim 0} Re_{in}^{-1.1955} x^{0.3748}. \tag{87}$$

The numbers δ_{00} and δ_{10} in (86) and (87) are given in Table 4.

We define the average heat transfer co-efficient $\bar{h}_\chi$ and the average Nusselt Number $\overline{Nu}_x$ in terms of the total heat transfer rate q over the bottom plate of length χ and unit width. As is common, the definitions are

$$\begin{aligned} q &\equiv \bar{h}_\chi(\chi \times 1)\,(\mathcal{T}_s(p_0) - \mathcal{T}_{w0}), \\ \overline{Nu}_x &\equiv \frac{\bar{h}_\chi \chi}{k_1}. \end{aligned} \tag{88}$$

Using the fact that q can be directly computed as

$$q = \int_0^\chi k_1 \frac{\partial \mathcal{T}_1}{\partial y}\bigg|_{y=0} dy \cong k_1 \Delta\mathcal{T} \int_0^x \frac{1}{\delta(x)} dx \quad , \tag{89}$$

we find (88)-(89) imply

$$\overline{Nu}_x = \int_0^x \frac{1}{\delta(x)} dx. \tag{90}$$

The correlation developed for $\overline{Nu}_x$, over $x \ge 0.01$, is given in the form

$$\overline{Nu}_x = \begin{cases} \overline{Nu}_{0x}\left(x, Re_{in}, \frac{Ja}{Pr_1}, \frac{\rho_2}{\rho_1}, \frac{\mu_2}{\mu_1}\right) & \text{for } Re_{in} \le Re_L \\ \overline{Nu}_{1x}\left(x, Re_{in}, \frac{Ja}{Pr_1}, \frac{\rho_2}{\rho_1}, \frac{\mu_2}{\mu_1}\right) & \text{for } Re_{in} \ge Re_L \end{cases} \tag{91}$$

where

$$\overline{Nu}_{0x} = n_{00}(\rho_2/\rho_1, \mu_2/\mu_1)\left(\frac{Ja}{Pr_1}\right)^{-0.2604} Re_{in}^{0.2023} x^{0.6607}, \tag{92}$$

and

$$\overline{Nu}_{1x} = n_{10}(\rho_2/\rho_1, \mu_2/\mu_1)\left(\frac{Ja}{Pr_1}\right)^{-0} Re_{in}^{1.1955} x^{0.6252} . \tag{93}$$

The numbers n_{00} and n_{10} above, for density and viscosity ratios in (67), are given in Table 4.

The correlation for the non-dimensional pressure π (x) for fully developed flow at the inlet (f_u given by (41)) is given in the form

$$\pi = \begin{cases} \pi_0\left(x, Re_{in}, \frac{Ja}{Pr_1}, \frac{\rho_2}{\rho_1}, \frac{\mu_2}{\mu_1}\right) & \text{for} \quad Re_{in} \le Re_L \\ \pi_1\left(x, Re_{in}, \frac{Ja}{Pr_1}, \frac{\rho_2}{\rho_1}, \frac{\mu_2}{\mu_1}\right) & \text{for} \quad Re_{in} \ge Re_U, \end{cases} \tag{94}$$

where

$$\pi_0 = \begin{cases} -\pi_{00}\left(\frac{Ja}{Pr_1}\right)^{-0.4766} Re_{in}^{-1.8515} x^{1.2241} & \text{for } 0.009 \le \frac{Ja}{Pr_1} \le 0.020 \\ -\pi_{01}\left(\frac{Ja}{Pr_1}\right)^{0.8482} Re_{in}^{-1.8515} x^{1.2241} & \text{for } 0.020 < \frac{Ja}{Pr_1} \le 0.045, \end{cases} \tag{95}$$

and

$$\pi_1 = \begin{cases} -\pi_{10}\left(\frac{Ja}{Pr_1}\right)^{0.7079} Re_{in}^{1.2358} x^{1.1357} & \text{for } 0.009 \le \frac{Ja}{Pr_1} \le 0.020 \\ -\pi_{11}\left(\frac{Ja}{Pr_1}\right)^{1.3058} Re_{in}^{2.3942} x^{1.1357} & \text{for } 0.020 < \frac{Ja}{Pr_1} \le 0.045. \end{cases} \tag{96}$$

The constants π_{00}, π_{01}, π_{10}, and π_{11} above, for density and viscosity ratios in (67), are given in Table 4.

The correlation for the non-dimensional average speed $u_{av}(x)$ is given in the form

$$u_{av}(x) = \begin{cases} u_{av0}\left(x, Re_{in}, \frac{Ja}{Pr_1}, \frac{\rho_2}{\rho_1}, \frac{\mu_2}{\mu_1}\right) & \text{for} \quad Re_{in} \le Re_L \\ u_{av1}\left(x, Re_{in}, \frac{Ja}{Pr_1}, \frac{\rho_2}{\rho_1}, \frac{\mu_2}{\mu_1}\right) & \text{for} \quad Re_{in} \ge Re_U, \end{cases} \tag{97}$$

where

$$u_{av0} = 1.0 - u_{00}(\rho_2/\rho_1, \mu_2/\mu_1)\left(\frac{Ja}{Pr_1}\right)^{1.024} Re_{in}^{-0.9804} x^{0.6832}, \tag{98}$$

and

$$u_{av1} = 1.0 - u_{10}(\rho_2/\rho_1, \mu_2/\mu_1)\left(\frac{Ja}{Pr_1}\right)^{1.3542} Re_{in}^{0.2974} x^{0.6837}. \tag{99}$$

The constants u_{00} and u_{10} above, for density and viscosity ratios in (67), are given in Table 4.

Also note that all of the constants, that depend on density and viscosity ratios, and which are listed in Table 4 can be correlated with respect to density ratio in the same fashion as the constants a_1 and $\hat{a}_1$ were correlated in equation (70). However such correlations will be *tentative* because of unavailability of data at different density and viscosity ratios. Therefore such correlations are not presented here.

9. DISCUSSION OF RESULTS

In Figure 2, we show a representative vapor velocity profile computed with the help of equations (38)-(39). The vertical dashed line corresponds to a uniform average speed of the type given by equation (37). The tiny solid line shown near the origin is for $u_1(x,y)$ over $0 \le y \le \delta(x)$, and it is the actual computed solution of the liquid velocity profile given by equation (30). Scaled up graphs for $u_1(x,y)$ show that the liquid velocity profile is essentially linear over all the flow situations specified by (67). This result is consistent with other film condensation results ([4], [11], etc.). It implies that interface shear $\tau_f(x)$ and bottom wall shear $\tau_w(x)$ are nearly equal over the range of flow parameters considered.

The choice of vapor velocity profile, whether it varies realistically, or merely has an average uniform value, does not affect the condensate motion significantly. As shown in Figure 3, the two choices of vapor velocity profile lead to less than 0.1 percent variations in film thickness and average speed over most x. The pressure variations also differ very little (within 5%), pressure gradients even less so than the pressures. Since the estimate on interfacial shear is affected only by film thickness and average speeds, it is concluded that the choice of vapor velocity profile in our solution method is not *significant* either for modeling the interfacial shear or the prediction of lower dimensional flow variables. Furthermore this result establishes that it is the interfacial shear which drives the liquid condensate and the requirement (16) of continuity of

tangential speeds has no noticeable impact.

The result in Figure 4 shows that inlet conditions, whether the incoming vapor is fully developed or nearly uniform, has only a second order effect (mostly on the pressure variations). Only the film thickness and average speed significantly influence the interfacial shear, and these variables, as shown, differ by less than 0.1 percent for the upper wall friction factor f_u corresponding to the two inlet conditions. The pressure variations, though important, are not significant in influencing interfacial shear unless it influences the average speed of the vapor or the film thickness. This does not happen because of the usual dominance (except for $\Delta\mathcal{T}$ near zero) of f over f_u. In the figure, the pressure gradients in the two flows are closer to each other than the absolute pressures. The kink in the pressure ratio curve is due to the fact that π_{II} (x) has a kink at $x \cong 17$ while π_I (x) does not. This is because f_u, for the choice in (42)-(43), changed from a laminar to a turbulent model near this transition point.

The result in Figure 5 establishes the value of the proposed model for interfacial shear as existing models give poor quantitative predictions. The Wallis Model (see (11.21b) on p. 461 of [18]), though not used in figure 5, can easily be verified to correspond to a friction factor f which is approximately one third of what is needed for agreement with experimental measurements. In Figure 6, we show the variation of the proposed friction factor f with distance x for two representative flow situations. For the flow situations considered, it is seen that the asymptotic form of friction is relevant only for $0 \leq x \leq \varepsilon$. Outside this zone, the friction factor variations are small. Although the variations with x are similar for both smooth and wavy interfaces, the correlations in (83)-(84) indicate that the value of the friction factor in the *wavy* interface flow regime increases more rapidly with vapor speed U and $\Delta\mathcal{T}$(i.e. Ja/Pr_1) than it does for the *smooth* interface flow regime. A plot of the values of physical shear stress τ_f in Figure 7 (see $[\tau_f]_{model}$ curve) shows that its value, unlike the non-dimensional friction f itself, decreases significantly with x because of a decreasing average speed of the vapor.

Figure 8, along with the correlation given in (85)-(87), establishes that film thickness decreases with increasing Reynolds number Re_{in} as well as with decreasing $\Delta\mathcal{T}$ (or Ja/Pr_1). However change in $\Delta\mathcal{T}$ in the *wavy* regime has a weak impact on film thickness as it is not even noticeable for the flow situation depicted by b and b(X) in Figure 10 or in the correlation given in (87). This means that a decrease in local wall heat flux $(q_1)_{y=0} = k_1\Delta\mathcal{T}/\delta(x)$ due to a decrease in $\Delta\mathcal{T}$ is nearly *proportional* to $\Delta\mathcal{T}$. However decrease in $\Delta\mathcal{T}$ significantly increases the average speed of the vapor (compare b(X) with b in Figure 9) and leads to decreased condensate mass flux. Through curves a, b, and c, Figure 9 shows the general trend of increase in average vapor speed with increasing Reynolds number.

Figure 10 shows some of the trends of pressure variations given in (95)-(96). Note that, in the smooth interface regime $\Delta\pi$ decreases with increasing Re_{in} (see case b and case c in Figure 10), however the physical pressure drop $\Delta p = \rho_2 U^2 \Delta\pi$ actually increases

The relative magnitude of forces shown in Figure 11 shows that the "kick-back" force associated with mass transfer (the third term on the left side of (36)) is typically very small compared to the other forces and can be ignored. It also shows that friction, pressure, and inertia

(associated with the right side of (36)) forces are comparable to each other. This shows that the friction force, through interfacial friction f, constrains vapor speed u_{av} (x) as much as mass balance does. This is the reason why ignoring momentum balance, as is done by Lu [15], does not lead to an acceptable model (compare the curves in Figure 7) for interfacial friction f. A slight kink in the value of forces at $x \cong 17$ is due to the fact that the upper wall friction factor f_u underwent a transition from laminar to turbulent. Recall that this did not affect the values of u_{av} (x) and δ (x) because the size of upper wall shear is still quite low compared to the size of interfacial shear.

The result in Figure 12 shows that typical pressure drops in the duct are too small to affect either the saturation temperature at the interface or the latent heat released at the interface. This is true for the entire parameter range given in (67).

The result in Figure 13 shows the general trend of decrease in condensate mass flux fraction with increase in inlet Reynolds number and associated increase in the average speed of the vapor.

We also find significantly increased heat transfer rates in the wavy regime. The near proportionality of heat transfer co-efficient in (93) to inlet Reynolds number Re_{in} is in agreement with known experimental correlations ([15], etc.) for high speed flows.

10. COMPARISON OF PREDICTED RESULTS WITH EXPERIMENTAL RESULTS

Note that β in section 7, was determined only from the requirement that for any flow situation in the experiment of Lu [15], the experimental and predicted heat transfer rate over $0 \le \chi \le L$ satisfy

$$q_{experiment} \cong q_{model} \cong k_1 w \Delta T \int_0^{L/h} \frac{1}{\delta(x)} dx, \tag{100}$$

for a plate of length L =0.899 m, a gap of height h = 0.025 m, and a plate of width w = 0.04 m.

However, in addition, Lu[15] gives film thickness $\Delta(\chi)$ measurements, for some smooth interface flows ($Re_{in} \le Re_L$), at five locations

$$\begin{gathered} \chi = 0.0508\text{m}, \quad \chi = 0.1524\text{m}, \quad \chi = 0.254\text{m}, \\ \chi = 0.4572\text{m}, \quad \chi = 0.8128\text{m}, \end{gathered} \tag{101}$$

and additional values of average heat transfer co-efficient $\bar{h}_\chi$ at

$$\chi = 0.2997\text{m}, \quad \chi = 0.5993\text{m}. \tag{102}$$

Since the modeling principle only insured that

$$\bar{h}_x\Big|_{\text{experimental}} = \bar{h}_x\Big|_{\text{model}} \tag{103}$$

for $x = 0.899$ m, we tested our correlations in section 9 with the additional measurements of Lu [15] for flow of R-113 and FC-72. The fluid properties can be found in [49] and [50]. We found that almost all the correlations given in section 8 are in agreement (within experimental error) with experimental data. A direct numerical simulation based on the proposed friction factor correlation is, of course, somewhat more accurate than correlations for the flow variables. For brevity, we show, in Table 5, a *sample* of the agreement obtained for flow situations involving R-113 and FC-72.

It is clear that this method can yield correlations of higher accuracy if the improved accuracy in experimental measurements *justify* seeking improved correlations.

11. CONCLUSIONS

We showed:

- The rigor and reliability of the proposed integral-differential scheme towards modeling of interfacial friction factor

We presented:

- A new and completely rigorous model for asymptotic friction factor at the point ($x \sim 0$) where condensation begins and condensation rate is high.
- Interfacial shear models for flow regimes involving both smooth and wavy interface.
- Qualitative understanding of the details of the flow fields including relative sizes of various types of forces that act on the vapor.
- Correlations for film thickness, pressure drops and heat transfer rates for both smooth and wavy interface flow regimes.

This work also identifies some research needs. These are:

- Greater accuracy, not just reliability, in experimental measurements. This can be used to propose friction factor models and other correlations of higher accuracy.
- Additional experiments with different fluids need to be done to provide correlations with respect to density and viscosity ratios.
- An experimental identification of laminar and turbulent vapor zones, near the lower limit of 9,500 in $(67)_5$, can help provide results in the low inlet Reynolds number (Re_{in}) zone.
- Additional experiments need to be done for a sharper identification of the transition from smooth to wavy interface regimes of flow.
- A correlation for downstream distance x_{upper} is needed so one can reliably state that liquid inertia and convection can be ignored for $x \leq x_{upper}$.

12. ACKNOWLEDGMENTS:

I thank Q. Lu and Professor N.V. Suryanarayana for keeping me informed on their experimental results. I thank my former M.S. student R. Kamath for assisting me on related earlier efforts which led to this work.

The work of Lu [15] and an earlier analysis [11] was supported in parts by NASA grant NAG 3-711.

13. APPENDICES

APPENDIX A

The functions appearing in (40) are defined as:

$$A_{22} \equiv -\frac{\rho_2}{\rho_1}(1-\delta(x))\,\delta(x), \tag{A.1}$$

$$A_{23} \equiv \frac{\rho_2}{\rho_1} u_{av}(x))\,\delta(x), \tag{A.2}$$

$$A_{32} \equiv 2(1-\delta(x))\,\delta(x), \tag{A.3}$$

$$A_{33} \equiv -u^2_{av}(x), \tag{A.4}$$

$$b \equiv \frac{\rho_2}{\rho_1}\{1-u_{av}(x)\,(1-\delta(x))\} \tag{A.5}$$

$$b_1 \equiv -\frac{3}{\delta^3(x)}\left[\frac{\mu_1}{\mu_2}\frac{1}{Re_2}b - \frac{1}{4}u^2_{av}(x)\,f\delta^2(x)\right], \tag{A.6}$$

$$b_2 \equiv \frac{Ja}{Pr_1}\frac{1}{Re_1}\frac{[T_s(\pi(x)) - T_w]}{\varphi_{fg}(\pi(x))}, \tag{A.7}$$

$$b_3 \equiv -b_1(1-\delta) - \frac{1}{2}u^2_{av}(x)\,(f+f_u) - \frac{\rho_1}{\rho_2}\dot{m}u_f\ , \tag{A.8}$$

where b_1 above is defined in terms of b, and b_3 is defined in terms of b_1 and the functions

$$\dot{m} \equiv \frac{Ja}{Pr_1}\frac{1}{Re_1}\frac{[T_s(\pi(x)) - T_w]}{\varphi_{fg}(\pi(x))}\frac{1}{\delta(x)}\ , \tag{A.9}$$

and

$$u_f \equiv \frac{\mu_2}{\mu_1} Re_2 \left[\frac{1}{2} u^2_{av}(x) f\delta(x) + (-b_1) \frac{\delta^2}{2} \right]. \tag{A.10}$$

The components g_1, g_2, and g_3 appearing in (45) are defined below:

$$g_1 \equiv b_1 \ , \tag{A.11}$$

$$g_2 \equiv \frac{b_2 A_{33} - b_3 A_{23}}{A_{22} A_{33} - A_{23} A_{32}} \ , \tag{A.12}$$

and

$$g_3 \equiv \frac{b_3 A_{22} - b_2 A_{32}}{A_{22} A_{33} - A_{23} A_{32}} \ . \tag{A.13}$$

The lack of sensitivity of the flow properties on the value of ε in (66) is demonstrated by the fact that if we consider a small interval $[\varepsilon_1, \varepsilon_2]$ in the vicinity of ε and define

$$f = \begin{cases} f_{asy} & \text{for} \quad x \le \varepsilon_1 \\ f_{regular} & \text{for} \quad x \ge \varepsilon_2 \\ (1 - \alpha(x))\, f_{asy} + \alpha(x)\, f_{regular} \ , \end{cases} \tag{A.14}$$

where

$$\alpha(x) \equiv (x - \varepsilon_1) / (\varepsilon_2 - \varepsilon_1) \qquad \text{for} \qquad \varepsilon_1 \le x \le \varepsilon_2, \tag{A.15}$$

then the solution utilizing (A.14)-(A.15) is indistinguishable from the solution utilizing (46) for $x \ge 0.1$. Here ε, ε_1, ε_2 take values between 10^{-5} to 10^{-3}.

Besides the proposed model in section 7, it is instructive to define some other common models used in Figure 5. The models are:

(i) Single Phase Model:

This model determines wall shear for fully developed turbulent flow between parallel plates and is defined in (41).

(ii) Shekriladze Model:

This model was proposed and used by Shekriladze, et al. ([5]) for condensing flows. The model is based on an adaptation of an exact solution of the Navier-Stokes equation for flow over a flat plate with suction.

$$f = f_{Shekriladze} = \frac{2\dot{m}(x)}{(\rho_2/\rho_1)\,(u_2)_{av}} \tag{A.16}$$

(iii) Mickley Model:

The Mickley model [23] is a semi-empirical proposal for flows in vertical tubes with suction at the walls. The model above behaves like the Shekriladze model in (A.16) for large $\dot{m}$ and like the single phase model f_0 in (41) for small $\dot{m}$. Here

$$f(x) = \frac{\phi_f \exp(\phi_f)}{\exp(\phi_f) - 1} f_0, \tag{A.17}$$

where

$$\phi_f \equiv \frac{2\dot{m}(x)}{(\rho_2/\rho_1)\,(u_2)_{av}(x)\,f_0(x)} \tag{A.18}$$

APPENDIX B

Under the notations

$$\begin{gathered}
c_1 \equiv C1, \quad c_2 \equiv C2, \quad \hat{c}_1 \equiv C1K, \quad \hat{c}_2 \equiv C2K, \quad \bar{c}_1 \equiv C1KK, \\
\bar{c}_2 \equiv C2KK, \quad k_1 \equiv K1, \quad \hat{k}_1 \equiv K1K, \quad \hat{k}_2 \equiv K2K, \quad \bar{k}_1 \equiv K1KK, \\
\bar{k}_2 \equiv K2KK, \quad \frac{Ja}{Pr_1} \equiv JAPR1, \quad \frac{\rho_2}{\rho_1} \equiv RHO21, \quad \frac{\mu_2}{\mu_1} \equiv MU21, \\
\frac{\rho_2 Uh}{\mu_2} \equiv Re_{in} \equiv RE2, \quad \frac{\rho_1 Uh}{\mu_1} \equiv Re_1 \equiv RE1, \quad B0 \equiv \frac{1}{Re_1}, \\
B1 \equiv \frac{Ja}{Pr_1}\frac{1}{Re_1}, \quad B2 \equiv 0.0
\end{gathered} \tag{B.1}$$

we find that computer generated double-precision fortran forms of the functions in (51) are as given below. Note that some of the *plus* signs on the left sides are *continuation marks* on the sixth column of a fortran expression.

```
C2 = 2.D0*B1/C1/RHO21-C1
```

(B.2)

```
C1K = -(-2.D0/3.D0*C1**2+C2*B1/RHO21/C1+1.D0/6.D0*C2/B0*C1**
+3+5.D0/6.D0*C1*C2+3.D0/2.D0*C2**2-2.D0/3.D0*B1/RHO21*MU21*RE2*C1*C
+2+1.D0/3.D0*B1/RHO21*C1**2/B0-2.D0/3.D0*B1/RHO21*MU21*RE2*C1**
+2)/(-1.D0-1.D0/C1*C2-B1/RHO21/C1**2)
```

(B.3)

```
C2K = -1.D0/3.D0*(-1.D0/2.D0*C2-B1/RHO21/C1+2.D0*B0/C1-B0/C1**2
+*C2+3.D0*B0/C1**4*C1K*C2-6.D0*B0/C1**3*C2**2+2.D0*B1/RHO21
+*MU21*RE2*B0/C1+2.D0*B1/RHO21*MU21*RE2*B0/C1**2*C2)/
+B0*C1**3
```

(B.4)

```
C1KK=((XPHI1/XPHI3)*XTPHI3-XTPHI1)/(XTPHI2-(XPHI2/XPHI3)*XTPHI3)
```

(B.5)

```
C2KK=-(XPHI1/XPHI3)-(XPHI2/XPHI3)*C1KK
```

(B.6)

where

```
XPHI1 = -2.D0/3.D0*B2*C1+4.D0/3.D0*B2*C2+4.D0/3.D0*B1/RHO21*MU21*R
+E2*B0/C1**3*C1K**2+12.D0*B0/C1**5*C1K**2*C2K+10.D0/3.D0*B1
+/RHO21*MU21*RE2*B0/C1**4*C1K**2*C2+2.D0*B1/RHO21*MU2
+1*RE2*B0/C1**3*C2K*C1K+12.D0*B0/C1**6*C1K**3*C2-24.D0*B
+0/C1**5*C1K**2*C2**2-2.D0/3.D0*B0/C1**4*C1K**2*C2+18.D0*B0
+/C1**4*C1K*C2**3-4.D0*B0/C1**2*C2*C2K-4.D0/3.D0*C2**2*B1/R
+HO21/C1-2.D0*B0/C1**2*C1K*C2-4.D0*B1/RHO21*MU21*RE2*B0/
+C1**3*C1K*C2**2+18.D0*B0/C1**3*C2K*C2**2-B1/RHO21*MU
+21*RE2*B0/C1**2*C1K*C2-4.D0*B1/RHO21*MU21*RE2*B0/C1*
+*2*C2*C2K-4.D0/3.D0*B1/RHO21/C1**3*C1K**2-4.D0*B0/C1**3*C1
+K*C2**2+B1/RHO21*MU21*RE2*B0/C1*C2**2+3.D0*B1/RHO21*
+MU21*RE2*B0/C1**2*C2**3-24.D0*B0/C1**4*C1K*C2*C2K+4.D0/
+3.D0*C2K*B1/RHO21/C1-B1/RHO21*MU21*RE2*B0/C1*C2K-8.D0*B
+0/C1**3*C2**4-2.D0*B0/C1*C2K+4.D0/3.D0*B0/C1**3*C1K**2+
+0.005941666667*1.D0/RE2**.25*C2+4.D0/3.D0*C2*B1/RHO21/
+C1**2*C1K+2.D0*B0/C1*C2**2+4.D0*B0/C1**2*C2**3-4.D0*B0/C1*
+*3*C2K**2
```

(B.7)

```
XPHI2 = 1.D0-6.D0*B0/C1**4*C2K-4.D0/3.D0*B1/RHO21*MU21*RE2*B
+0/C1**2-7.D0/3.D0*B1/RHO21*MU21*RE2*B0/C1**3*C2-12.D0*B0/C
+1**5*C1K*C2+12.D0*B0/C1**4*C2**2+2.D0/3.D0*B0/C1**3*C2+4.D0/3.D0
+*B1/RHO21/C1**2-4.D0/3.D0*B0/C1**2
```

(B.8)

```
XPHI3 =(-6.D0*B0/C1**4*C1K+8.D0*B0/C1**3*C2-1.D0*B1/RH
+O21*MU21*RE2*B0/C1**2)
```

(B.9)

```
XTPHI1 = C2K-2.0000000D0*B0/C1**2*C1K-9.D0*B0/C1**4
+*C1K*C2K-9.D0*B0/C1**5*C1K**2*C2+15.D0*B0/C1**4*C1K*C2
+**2+9.D0*B0/C1**3*C2*C2K+4.000000D0*B0/C1**3*C1K*C2
+-7.D0/2.D0*B1/RHO21*MU21*RE2*B0/C1**3*C1K*C2+.03565
+0000D0*1.D0/RE2**.25D0-2.D0*B1/RHO21*MU21*RE2*B0/C1*
+*2*C1K+1.D0*B1/RHO21/C1**2*C1K-3.D0*B0/C1**3*C2**3+1.D0
+*B1/RHO21*MU21*RE2*B0/C1**2*C2**2+2.0000000D0*B0+
+B2-3.D0/2.D0*B1/RHO21*MU21*RE2*B0/C1**2*C2K+2.D0*B1/RHO21*
+MU21*RE2*B0-2.0000000D0*B0/C1**2*C2**2+3.D0*B0/C1**2
+*C2K+1.5000000D0*B1/RHO21*MU21*RE2*C2*B0/C1-1.D0*B1
+/RHO21
```

(B.10)

```
XPHI3 =(-6.D0*B0/C1**4*C1K+8.D0*B0/C1**3*C2-1.D0*B1/RH
+O21*MU21*RE2*B0/C1**2)
```

(B.11)

```
XTPHI1 = C2K-2.0000000D0*B0/C1**2*C1K-9.D0*B0/C1**4
+*C1K*C2K-9.D0*B0/C1**5*C1K**2*C2+15.D0*B0/C1**4*C1K*C2
```

```
+**2+9.D0*B0/C1**3*C2*C2K+4.000000D0*B0/C1**3*C1K*C2
+-7.D0/2.D0*B1/RHO21*MU21*RE2*B0/C1**3*C1K*C2+.03565
+0000D0*1.D0/RE2**.25D0-2.D0*B1/RHO21*MU21*RE2*B0/C1*
+*2*C1K+1.D0*B1/RHO21/C1**2*C1K-3.D0*B0/C1**3*C2**3+1.D0
+*B1/RHO21*MU21*RE2*B0/C1**2*C2**2+2.0000000D0*B0+
+B2-3.D0/2.D0*B1/RHO21*MU21*RE2*B0/C1**2*C2K+2.D0*B1/RHO21*
+MU21*RE2*B0-2.0000000D0*B0/C1**2*C2**2+3.D0*B0/C1**2
+*C2K+1.5000000D0*B1/RHO21*MU21*RE2*C2*B0/C1-1.D0*B1
+/RHO21
```

(B.12)

```
XTPHI2 = 3.D0*B0*C2/C1**4
```

(B.13)

```
XTPHI3 = 3.D0*B0/C1**3
```

(B.14)

```
K1 = 6.D0*B0/C1**4*C1K*C2+6.D0*B0/C1**3*C2K-6.D0*B0/C1**2
+*C2-12.D0*B0/C1**3*C2**2
```

(B.15)

```
K1K = 3.D0*B0/C1**2*(-2.D0*C1KK/C1+3.D0*C1K**2/C1**2)+B2+
+3.D0*B0/C1**2*C2K+6.D0*B0/C1**3*C1K*C2+3.D0*B0/C1**3*(-2.D0*C
+1KK/C1+3.D0*C1K**2/C1**2)*C2-3.D0*B0/C1**2*(-3.D0*C1KK/C1+
+6.D0*C1K**2/C1**2)+6.D0*B0/C1**3*C2*C2K+3.D0*B0/C1**3*C2KK
++9.D0*B0/C1**4*C1K**2-3.D0*B0/C1**3*(-3.D0*C1KK/C1+6.D0*C1K**
+2/C1**2)*C2+3.D0*B0/C1**2*C2**2+12.D0*B0/C1**4*C1K*C2**
+2+3.D0*B0/C1**3*C2**3-3.D0*B0/C1**3*C1KK-9.D0*B0/C1**4*C1K
+*C2K
```

(B.16)

```
K1KK = 8.D0*B0/C1**4*C1KK*C2**2-12.D0*B0/C1**5*C1K**2*
+C2**2-12.D0*B0/C1**5*C1K*C1KK*C2+12.D0*B0/C1**6*C1K**3*
+C2-6.D0*B0/C1**4*C1KK*C2K+12.D0*B0/C1**5*C1K**2*C2K-8.D0*B
+0/C1**4*C1K*C2*C2K-4.D0*B0/C1**2*C2*C2K-4.D0*B0/C1**3*C
+1K*C2K-6.D0*B0/C1**4*C1K**2*C2-4.D0*B0/C1**4*C1K*C2**3-
+4.D0*B0/C1**3*C2**2*C2K-4.D0*B0/C1**3*C1K*C2**2-6.D0*B0/C1
+**4*C1K*C2KK+2.D0*B0/C1**2*C2KK+4.D0*B0/C1**3*C2*C2KK+4.D0
+*B0/C1**3*C2*C1KK
```

(B.17)

The function Ψ in (52) is defined through

$$\Psi \equiv F1 + F2, \tag{B.18}$$

where

e

```
F1= 2.D0/3.D0*C2*B2+C2KK+4.D0/3.D0*B0*C1-2.D0/3.D0*B1/RHO21*C1
++10.D0*B0/C1**4*C1KK*C2**2-18.D0*B0/C1**5*C1K**2*C2**2+6.D0*B0
+/C1**3*C2*C2KK+6.D0*B0/C1**3*C2**2*C2K-2.D0*B0/C1**3*C2
+K**2+6.D0*B0/C1**4*C1K*C2**3-16.D0*B0/C1**4*C1K*C2*C2K-
+6.D0*B0/C1**4*C1KK*C2K+12.D0*B0/C1**5*C1K**2*C2K+2.D0*B0/C
+1**2*C2KK+B1/RHO21*MU21*RE2*C2*B0-6.D0*B0/C1**4*C1K*
+C2KK-4.D0/3.D0*B0/C1*C2**2+0.02376666667D0*1.D0/RE2*
+*.25*C1+4.D0/3.D0*B1/RHO21*MU21*RE2*B0*C1-4.D0*B0/C1**3*C2
```

```
+K*C1K+4.D0/3.D0*B0/C1**2*C2K*C2+4.D0/3.D0*B0/C1**3*C1K**2-12.D0*
+B0/C1**5*C1K*C1KK*C2+12.D0*B0/C1**6*C1K**3*C2+2.D0/3.D0*B1
+/RHO21*MU21*RE2*C2**2*B0/C1-5.D0/3.D0*B1/RHO21*MU21*RE2
+*B0/C1**2*C2K*C2-14.D0/3.D0*B0/C1**4*C1K**2*C2+4.D0/3.D0*C2*B
+0/C1**2*C1K
```

(B.19)

```
F2=0.D0+8.D0/3.D0*B0/C1**3*C1KK*C2-4.D0/3.D0*B1/RHO21*MU2
+1*RE2*B0/C1**2*C1KK+2.D0*B1/RHO21*MU21*RE2*B0/C1**3*
+C2K*C1K-B1/RHO21*MU21*RE2*B0/C1**2*C2KK+4.D0/3.D0*B1/RH
+O21*MU21*RE2*B0/C1**3*C1K**2-7.D0/3.D0*B1/RHO21*MU21*RE
+2*B0/C1**3*C1KK*C2+2.D0/3.D0*B1/RHO21/C1**2*C1KK-2.D0/3.D0*B1
+/RHO21/C1**3*C1K**2-4.D0/3.D0*B0/C1**2*C1KK-2.D0*B0/C1**3*
+C2**4-0.017825000D0*1.D0/RE2**.25*C2+4.D0/3.D0*B0
+/C1*C2K-2.D0/3.D0*B1/RHO21*MU21*RE2*C2K*B0/C1-2.D0/3.D0*B1/RH
+O21*MU21*RE2*B0/C1**2*C2*C1K+B1/RHO21*MU21*RE2*B0
+/C1**2*C2**3+4.D0/3.D0*B0/C1**3*C1K*C2**2-5.D0/3.D0*B1/RHO21*
+MU21*RE2*B0/C1**3*C1K*C2**2+10.D0/3.D0*B1/RHO21*MU21*RE
+2*B0/C1**4*C1K**2*C2
```

(B.20)

and the terms appearing in (B.19)-(B.20) are as defined in (B.1)-(B.17).

14. REFERENCES:

1. W. Nusselt, "Die Oberflächenkondesation des Wasserdampfes," *Z. Ver. Dt. Ing. 60*(27), 541-546, (1916).
2. W.M. Rohsenow, "Heat Transfer and Temperature Distribution in Laminar Film Condensation,"*Transactions ASME*, 78, 1645-1648, (1956).
3. E.M. Sparrow and J.L. Gregg, "A Boundary Layer Treatment of Laminar Film Condensation," *ASME J. Heat Transfer*, 81, 13-18, (1959).
4. J.C.Y. Koh, "Film Condensation in a Forced-Convection Boundary-Layer Flow," *Int. J. Heat Mass Transfer,* 5, 941-954 (1962).
5. I.G. Shekriladze and V.I. Gomelauri, "Theoretical Study of Laminar Film Condensation of Flowing Vapour," *Int. J. Heat Mass Transfer*, Vol. 9, pp. 581-591, (1966).
6. M.M. Chen, "An analytical study of laminar film condensation, Part I-flat plates," *J. of Heat Transfer*, Series C, 83, pp. 48-55, (1961).
7. T. Fujii and H. Uehara, "Laminar Filmwise Condensation on a Vertical Surface," *Int. J. of Heat and Mass Transfer*, 15, pp. 217-233, (1972).
8. H. Honda and T. Fujii, "Condensation of Flowing Vapor on a Horizontal Tube Numerical Analysis as a Conjugate Heat Transfer Problem," *Trans. ASME, J. Heat Transfer*, Vol. 106, pp. 841-848, (1984).
9. F.G. Carpenter and A.P. Colburn, "The Effect of Vapor Velocity on Condensation Inside Tubes," *Proceedings of the General Discussion of Heat Transfer, The Institute of Mechanical Engineers and the ASME*, pp. 20-26, July (1951).
10. I.Y. Chen and G. Kocamustafaogullari, "Condensation Heat Transfer Studies for Stratified, Co-current Two-Phase flow in Horizontal Tubes," *Int. J. Heat Mass Transfer*, Vol. 30,

No. 6, pp. 1133-1148, (1987).
11. A Narain and Y. Kizilyalli: "Pressure Driven Flow of Pure Vapor Undergoing Laminar Film Condensation Between Parallel Plates," *International Journal of Non-Linear Mechanics*, Vol. 26, No. 5, pp. 501-520, (1991).
12. A. Narain, "Interfacial Shear Modeling and Flow Predictions for Internal Film Condensation Flows," Fluid Mechanics Phenomena in Microgravity, ASME-AMD Vol. 154 and FED Vol. 142, pp. 23-38, (1992).
13. M. Soliman, J.R. Schuster and P.J. Berenson, "A General Heat Transfer Correlation For Annular Flow Condensation," *J. Heat Transfer*, 90, 267-276, (1986).
14. J.D. Ford and A. Lekic, "Rate of Growth of Drops During Condensation," *Int. J. Heat Mass Transfer*, 16, 61-66, (1973).
15. Q. Lu, "An Experimental Study of Condensing heat Transfer with film condensation in a Horizontal Rectangular Duct," *Ph.D. Thesis*, Michigan Technological University, Houghton, Michigan, (1992).
16. J.M. Delhaye, "Jump Conditions and Entropy Sources in Two-phase Systems; Local Instant Formulation," *Int. J. of Multiphase Flow*, 1, 395-409, (1974).
17. M. Ishii, Thermo Fluid Dynamic Theory of Two-Phase Flow, Eyerolles, (1975).
18. V.P. Carey, Liquid-Vapor Phase-Change Phenomena, Series in Chemical and Mechanical Engineering, Hemisphere Publishing Corporation, (1992).
19. W.M. Rohsenow, "Status of and Problems in Boiling and Condensation Heat Transfer," in *Progress in Heat and Mass Transfer* edited by Hetsroni, Sideman, and Hartnett, Pergaman Press, Vol. 6, pp. 1-144, (1972).
20. R.W. Lockhart and R.C. Martinelli, "Proposed Correlation of Data for Isothermal Two Phase, Two Component Flow in Pipes," *Chem. Engng. Progress*, 45, No. 1, pp. 39-48, (1949).
21. L.P. Wang, V.P. Carey, R. Grief, and D. Abdollahian, "Experimental Simulation and Analytical Modeling of Two-Phase Flow Under Zero Gravity Conditions," *Int. J. Multiphase Flow*, Vol. 16, No. 3, pp. 407-419, (1990).
22. R.B. Kinney and E.M. Sparrow, "Turbulent Flow, Heat Transfer, and Mass Transfer in a Tube with Surface Suction," *ASME J. of Heat Transfer*, 92(1), pp. 117-124, (1970).
23. H.S. Mickley, "Heat, Mass, and Momentum Transfer for Flow Over a Flat Plate With Blowing or Suction," NACA-TN-3208 (1954).
24. G.B. Wallis, "Annular Two-Phase Flow, Part 2-Additional Effects," *J. Basic Engng.*, 92, pp. 73-82, (1970).
25. G.F. Hewitt and A.H. Govan, "Phenomena and Prediction in Annular Two-Phase Flow," *Advances in Gas-Liquid Flows* 1990, edited by J.H. Kim, V.S. Rohtagi and A. Hashemi, *ASME FED*- Vol. 99 and HTD-Vol. 155, pp. 41-55, (1990).
26. W.M. Rohsenow, J.H. Webber, and A.T.Ling, "Effect of Vapor Velocity on Laminar and Turbulent Film Condensation," *Trans. Am. Soc. Mech. Eng., Ser. C, J. Heat Transfer*, 78, pp. 1637-1643, (1956).
27. A.E. Dukler, "Fluid Mechanics and Heat Transfer in Vertical Falling Film Systems," *Chem. Eng. Prog. Symp. Ser.* 56, pp. 1-10, (1960).
28. F. Blangetti, "Lokaler Wärmeübergang bei der Kondensation mit überlagerter Konvektion in vertikalen Rohr," Diss. Univ. Karlsruhe, (1979).
29. S.L. Chen, F.M. Gerner, and C.L. Tien, "General Film Condensation Correlations," *Exp. Heat Transfer*, vol. 1, pp. 93-107, 1987.
30. K. Stephan, Heat Transfer in Condensation and Boiling (English Edition), International

Series in Heat and Mass Transfer, Springer Verlag, (1992).
31. J.M. Delhaye, "Two Phase Flow Patterns," Chapter 1 in *Two Phase Flow and Heat Transfer in the Power and Process Industries*, edited by A.E. Bergles, J.G. Collier, J.M. Delhaye, G.F. Hewitt and F. Mayinger, Hemisphere Publishing (1981).
32. K.J. Bell, J. Taborek and F. Fenoglio, "Interpretation of Horizontal In-Tube Condensation Heat Transfer Correlations with a Two-Phase flow Regime Map," *Chem. Engng. Prog. Symposium Series*, 66, (102), pp. 150-163, (1970).
33. H. Schlichting, Boundary Layer Theory, Sixth Edition, McGraw Hill, (1968).
34. J.E.A. John, and W.L. Haberman, Introduction to Fluid Mechanics, Prentice Hall, (1988).
35. W.J. Minkowycz and E.M. Sparrow, "Condensation Heat Transfer in the presence of non-condensables, Interfacial Resistance, Superheating, Variable Properties, and Diffusion," *Int. J. Heat Mass Transfer*, **9**, pp. 1125-1144, (1966).
36. C.Y. Wang and C.J. Tu, "Effects of Non-Condensable Gas on Laminar Film Condensation in a Vertical Tube," *Int. J. Heat Mass Transfer*, 31, 2339-2345 (1988).
37. B.C. Khoo, A.T. Patera, and A.A. Sonin, "Direct Numerical Simulation of Pure Vapor Condensation At a Turbulent Liquid Interface: An Extracted-Subdomain Approach," in *Heat Transfer With Phase Change*, edited by I.S. Habib and R.J. Dallman, *ASME HTD*-Vol. 114, pp. 39-50, (1989).
38. L.F. Moody, "Friction factors for Pipe Flow," ASME *Trans.*, Vol. 66, pp. 671-684, (1944).
39. N.Z. Azer, L.V. Abis, and T.B. Swearingen, "Local Heat Transfer Coefficients during Forced Convection Condensation inside Horizontal Tubes," *Trans. ASHRAE*, 77, 182-201, (1971).
40. W.W. Akers, and H.E. Rosson, "Condensation inside a Horizontal Tube," *Chem. Eng. Prog. Symp. Series, Heat Transfer*, Storrs, Vol. 56, No. 30, 145-149, (1960).
41. D.P. Traviss, W.M. Rohsenow, and A.B. Baron, "Forced-Convection Condensation inside Tubes: A Heat Transfer Equation for Condenser Design," *ASHRAE Trans.* Vol. 79, Part 1, 157-165, (1973).
42. M.M. Shah, "A General Correlation for Heat Transfer during Film Condensation inside Pipes," *Int. J. Heat Mass Transfe*r, 22, pp. 547-556, (1979).
43. K. Lucas and B. Moser, "Laminar Film Condensation of Pure Vapors in Tubes," *Int. J. of Heat and Mass Transfer*, 22, 431-435 (1979).
44. F.M. White, Viscous Fluid Flow, McGraw Hill, (1974).
45. M.D. Greenberg, Foundations of Applied Mathematics, Prentice Hall, (1978).
46. G.L. Baker and J.P. Gollub, Chaotic Dynamics: An Introduction, Cambridge University Press, (1992).
47. J.H. Linehan, M. Petrick, and M.M. El-Wakil, M.M, "On the Interface Shear Stress in Annular Flow Condensation," *Journal of Heat Transfer,* pp 450-452, August., (1969).
48. R.J. Jensen, and M.C. Yuen, "Local heat and Mass Transfer Correlation in Horizontal Stratified concurrent Flow," *Proc. 7th Int. Heat Transfer Conference,* Munichen, pp. 95-100, (1982).
49. *ASHRAE Handbook*, Fundamentals SI Edition, American Society of Heating, Refrigeration and Air-Conditioning Engineers, Inc., Atlanta, GA (1985).
50. 3M, *Fluorinert*$^{T.M.}$ *Electronic Liquids*, Handbook (1989).

15. FIGURES

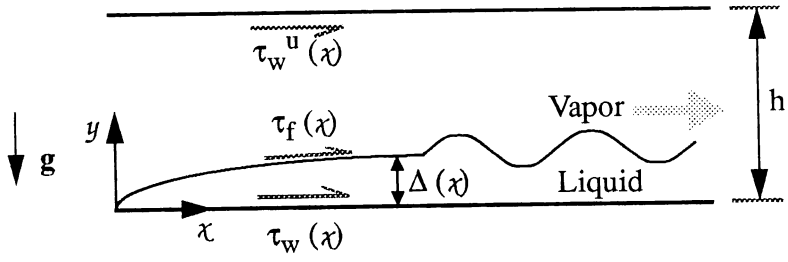

FIGURE 1: The geometry of the flow is indicated above. In the figure $\tau_w^u(x)$, $\tau_f(x)$, and $\tau_w(x)$ respectively indicate the values of shear stresses at the upper wall, the interface, and the bottom plate.

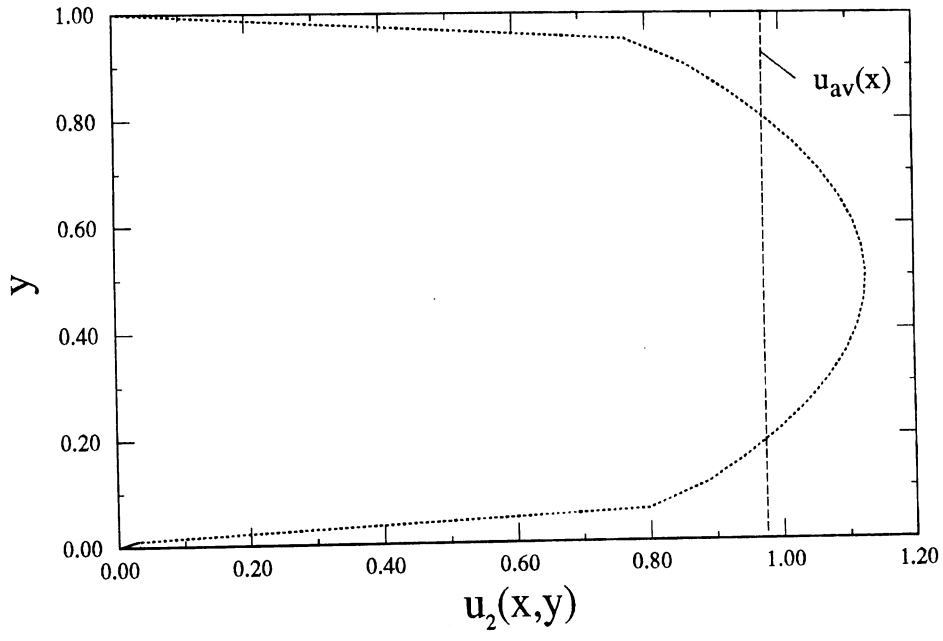

Figure 2: The above vapor velocity profile $u_2(x,y)$, shown by a dotted line, is the computed solution at x = 15 for the flow of R-113 at conditions specified by case # 7 in Table 1. The form of vapor velocity profile chosen in the computation is given by equations (38)-(39). At x=15, the film thickness δ (x) is 0.01118 and dimensionless interfacial speed u_f (x) is 0.03263.

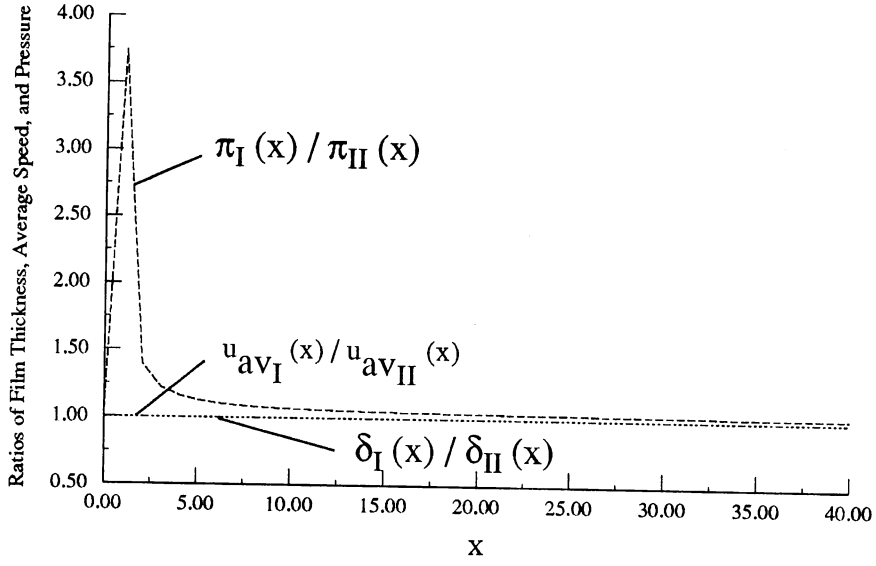

Figure 3: The above film thickness, average speed, and pressure ratios are *typical* values represented by a computed solution for flow of R-113 at conditions specified by case # 7 of Table 1. The computed solutions $\delta_I(x)$, $u_{avI}(x)$, and $\pi_I(x)$ above correspond to a uniform vapor velocity profile given by equation (37). The computed solutions $\delta_{II}(x)$, $u_{avII}(x)$, and $\pi_{II}(x)$ correspond to a more realistic vapor velocity profile given by equations (38)-(39).

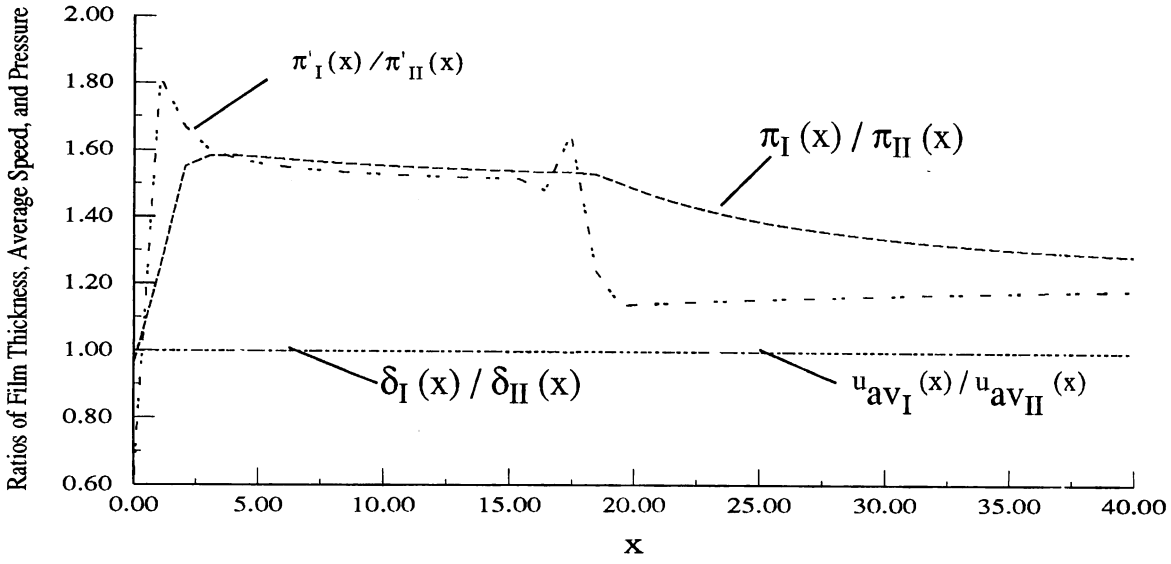

Figure 4: The above film thickness, average speed, and pressure ratios are *typical* values represented by a computed solution for flow of R-113 at conditions specified by case # 7 of Table 1. The computed solutions $\delta_I(x)$, $u_{avI}(x)$, $\pi_I(x)$and $\pi'_I(x)$ above correspond to upper wall friction factor f_u given by equation (41). The computed solutions $\delta_{II}(x)$, $u_{avII}(x)$, $\pi_{II}(x)$ and $\pi'_{II}(x)$ correspond to upper wall friction factor f_u given by equations (42)-(43).

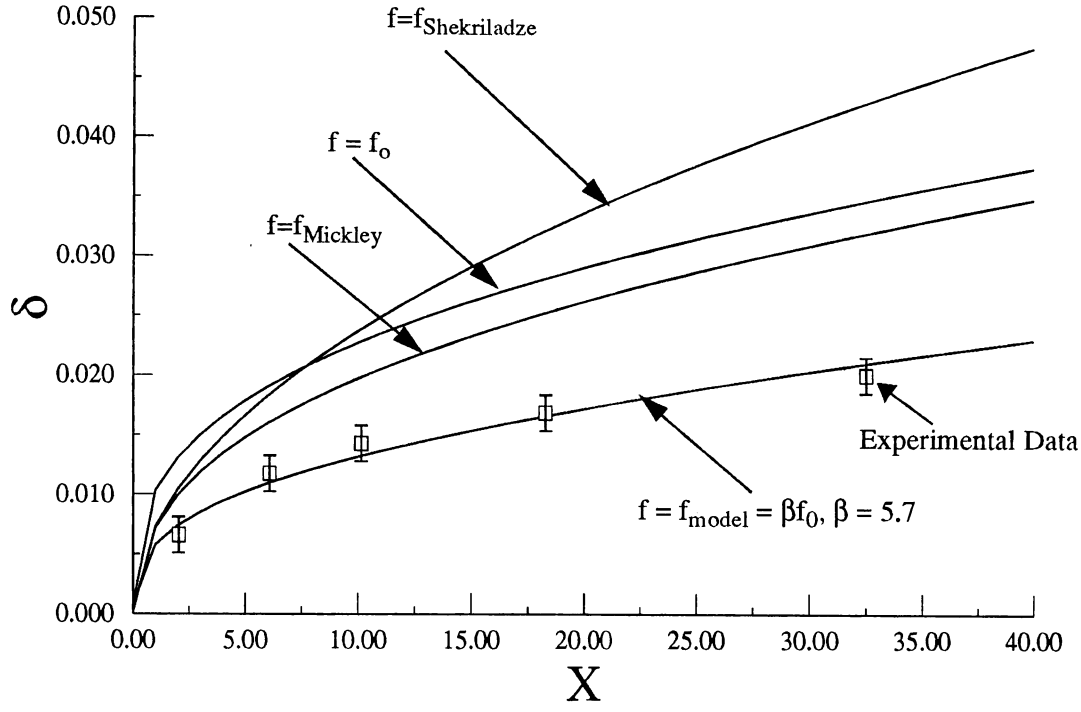

Figure 5: The above figure compares the film thickness variations predicted by some of the commonly used models and the proposed model (see section 7) with experimental measurements ([15]). All the common models shown above are defined in Appendix A. The comparisons above are for smooth interface flow of R-113 as specified by case # 9 of Table 1.

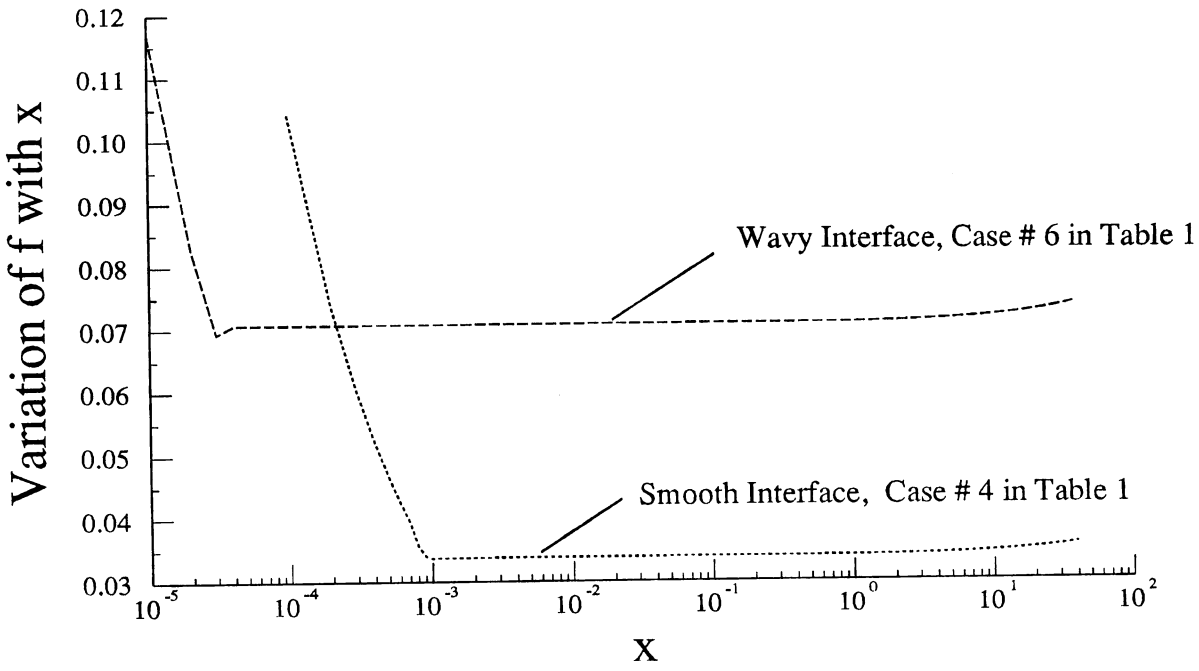

Figure 6: The variations of interfacial friction factor f is shown for two *typical* flow situations specified on the curves.

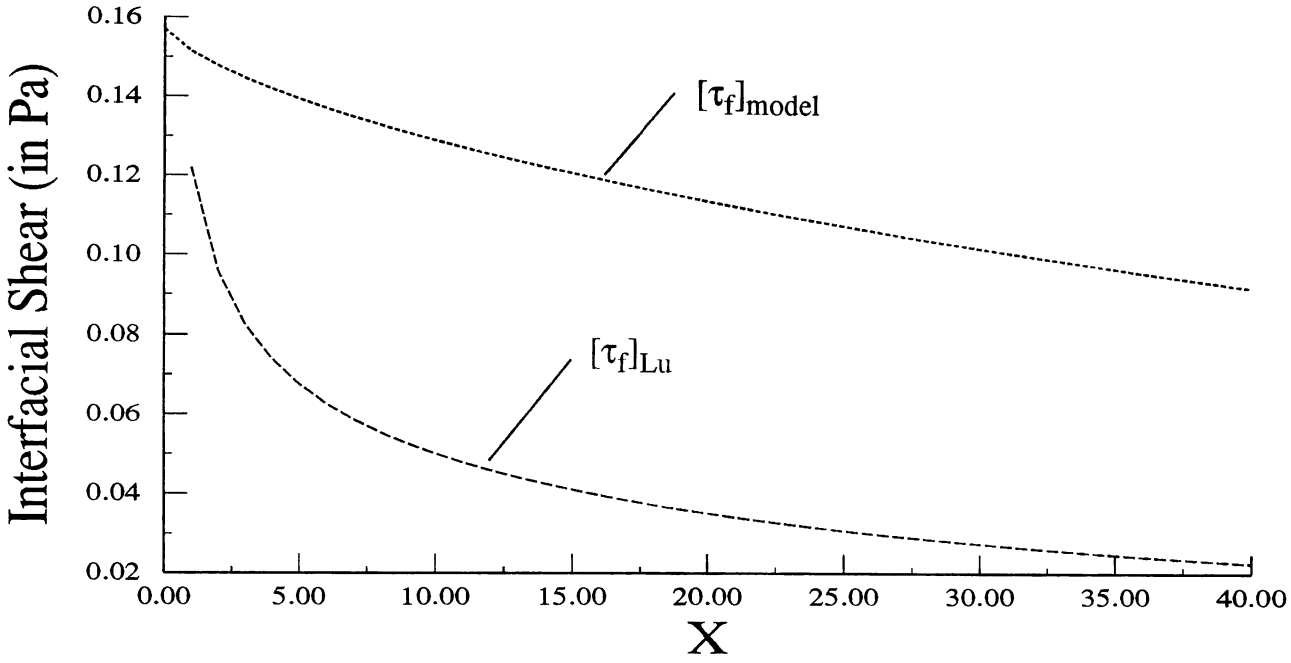

Figure 7: The physical values of interfacial shear are shown above for the proposed model and a model of Lu [15] for a representative flow of R-113 specified by case # 2 of Table 1. The prediction from Lu's model, depending on the flow situation, varies from our model anywhere in the range of ±10% to ±600%.

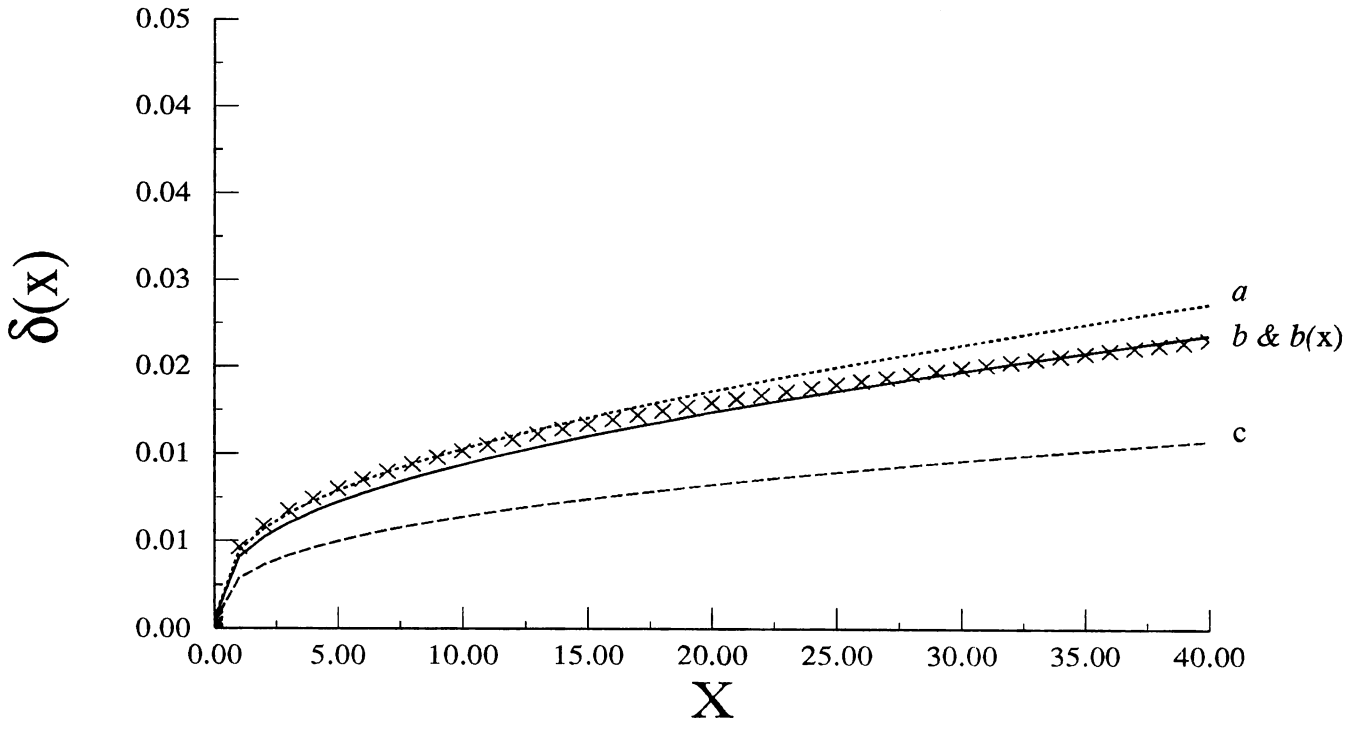

Figure 8: The decreasing film thickness represented by curves a, b, and c above correspond to increasing Reynolds numbers at a fixed temperature difference of $\Delta\mathcal{T} \cong 30°C$. The cases a, b, and c are respectively specified by case #s 1,2, and 5 of Table 1. The curve b(X), represented by the Xs, is for a flow (case # 8 in Table 1) which is identical to b (case # 2 in Table 1) except that it has a smaller $\Delta\mathcal{T}$ of 10°C.

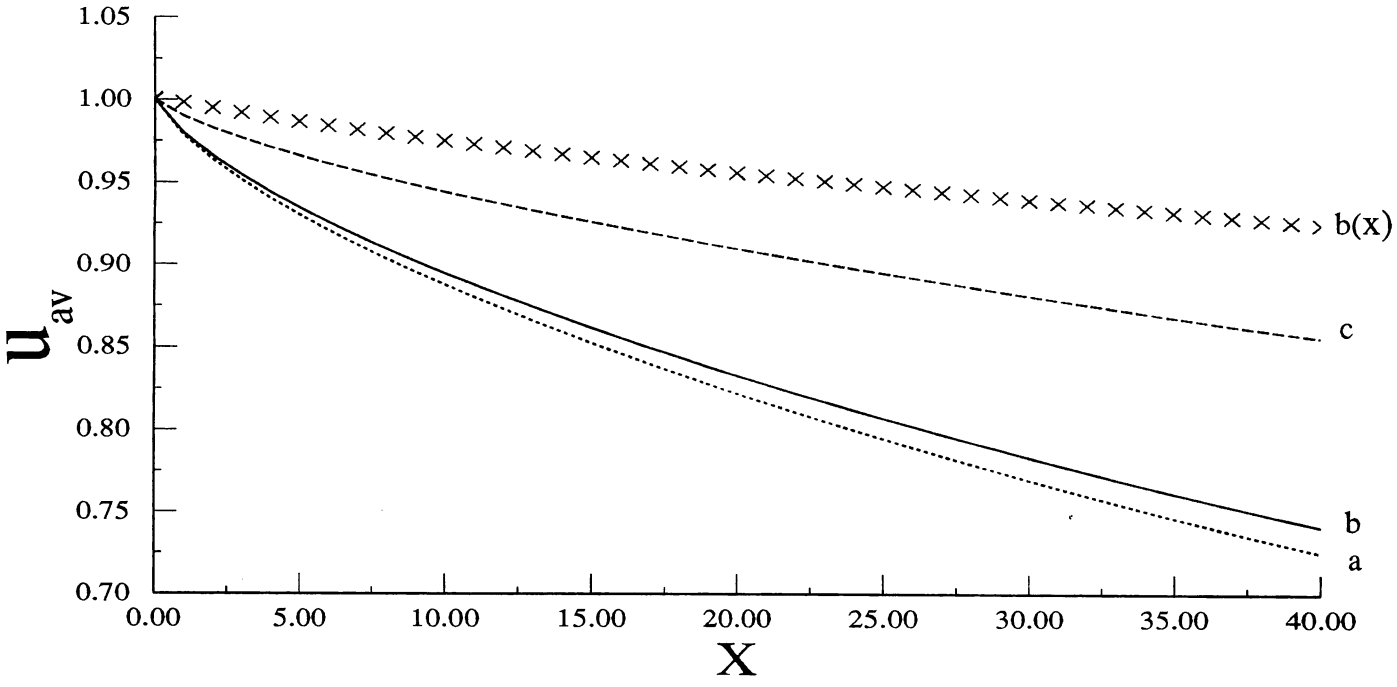

Figure 9: The increasing average speed represented by curves a, b, and c above correspond to increasing Reynolds numbers at a fixed temperature difference of $\Delta\mathcal{T} \cong 30°C$. The cases a, b, and c are respectively specified by case #s 1, 2, and 5 of Table 1. The curve b(X), represented by the Xs, is for a flow (case # 8 in Table 1) which is identical to b (case # 2 in Table 1) except that it has a smaller $\Delta\mathcal{T}$ of 10°C.

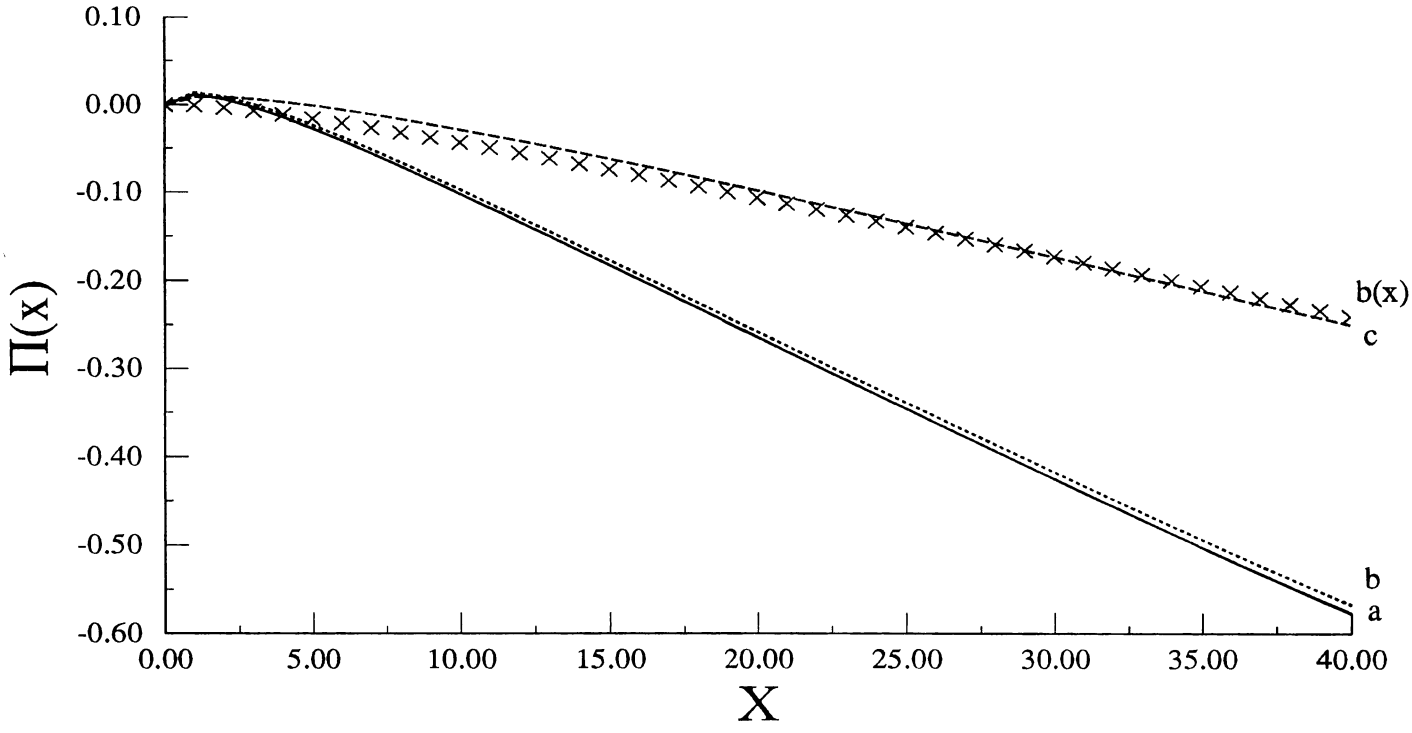

Figure 10: Curves b and c above represent decreasing $\Delta\pi \equiv \pi(0)-\pi(x)$ due to increasing Re_{in} at a fixed $\Delta\mathcal{T}$. The curves a, b, and c correspond to case # s 1, 2, and 5 specified in Table 1. The curves b and b(x) correspond to case #s 2 and 8 in Table 1.

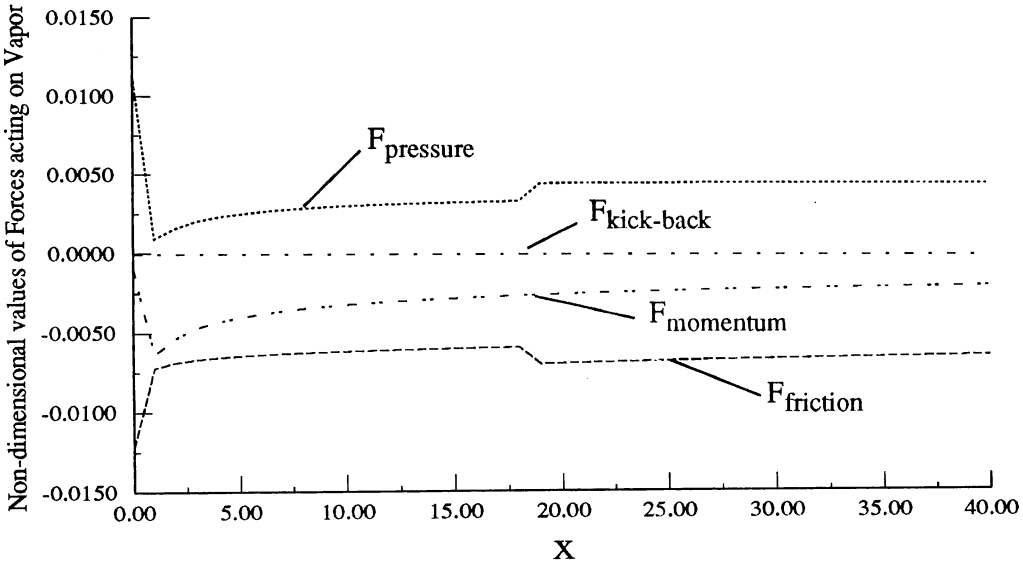

Figure 11: The above figure depicts the relative magnitudes of various components of forces acting on the vapor for a representative flow of R-113 specified by case # 7 of Table 1 with f_u as specified by equations (42)-(43).

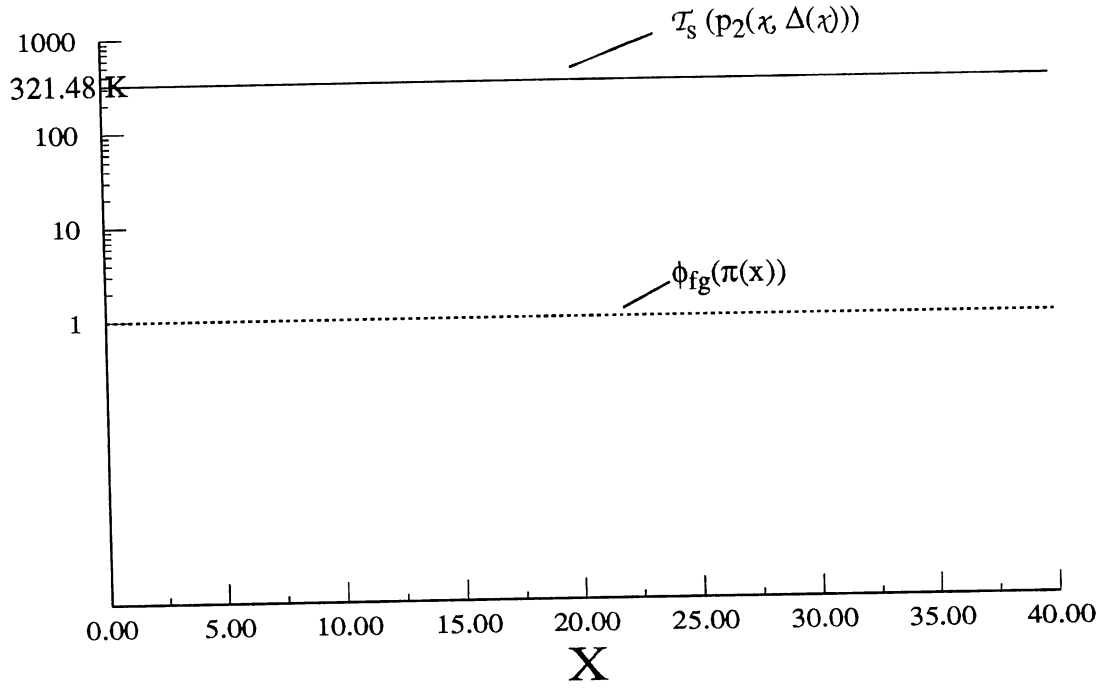

Figure 12: The plot above indicates the insignificant influence of pressure variation on saturation temperature $\mathcal{T}_s(p)$ and latent heat released (see equation (19) for a definition of ϕ_{fg}) at the interface. The results above are for a representative flow of R-113 specified by case # 2 of Table 1.
Also note that the functions $T_s(\pi)$ (see definition in (17)) and $\phi_{fg}(\pi)$ used in determining the above curves are determined by curve fitting the standard thermodynamic data given in [49].

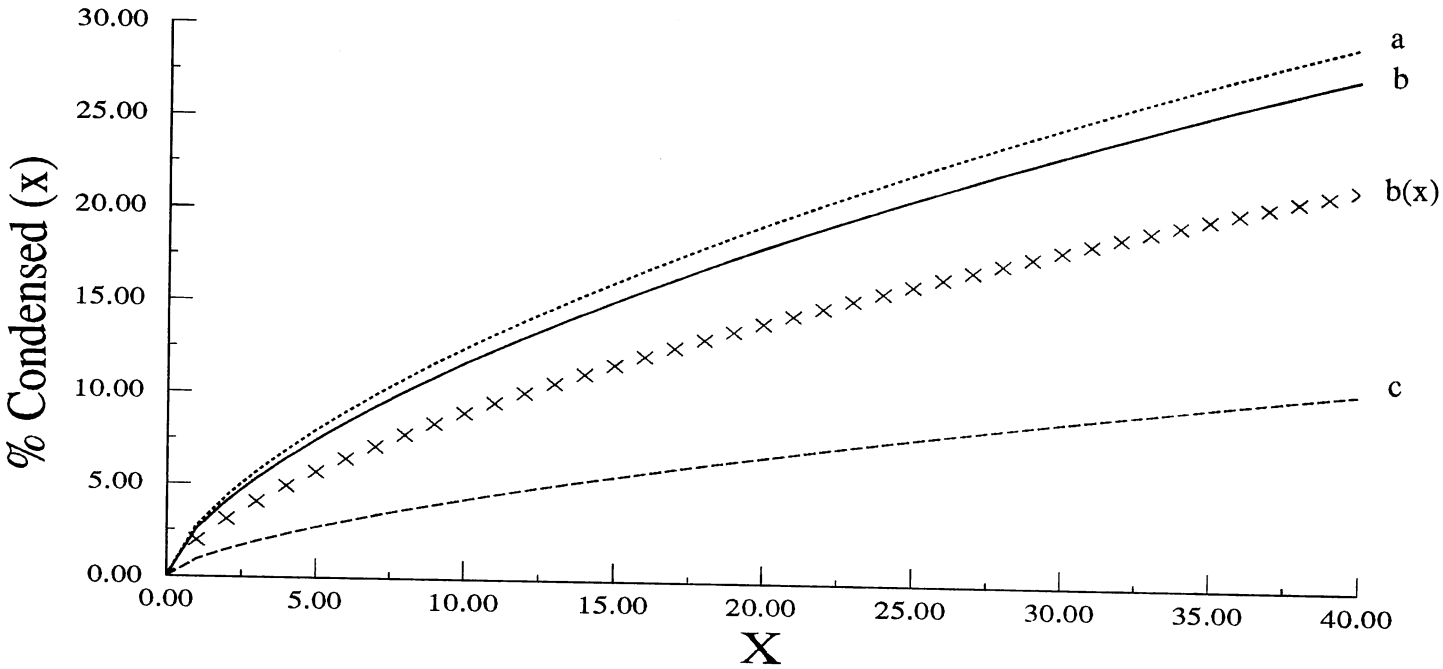

Figure 13: The variable % Condensed (x) above is hundred times the ratio of fluid mass flux to total mass flux (often called *quality*). The cases a, b, and c are respectively specified by case #s 1,2, and 4 of Table 1. The curve b(x), represented by the Xs, is for a flow (case # 8 in Table 1) which is identical to b (case # 2 in Table 1) except that it has a smaller ΔT of 10°C.

16. TABLES

Table 1: The Table below specifies the sample flow conditions used in the Figures.The fluid is R-113 and all the parameters can be computed from properties listed in [49]. Liquid properties were evaluated at a *reference temperature* of $\Delta T/2+T_{w0}$ and vapor properties were computed at saturation temperature. The gap between plates is h = 0.025 m.

Case #	Expt. Run # in Lu [15]	Average Inlet Speed, U (In m/s)	Sat. Temp. of Vapor $T_s(p_0)$ (In K)	Inlet Press. p_0 (In MPa)	Wall Temp. T_w (In K
1	226	0.72	321.32	0.1033	290.04
2	184	0.82	321.48	0.1039	290.78
3	207	0.84	322.29	0.1067	290.67
4	196	1.03	321.22	0.1030	290.67
5	247	2.20	320.55	0.1007	290.30
6	234	3.92	320.56	0.1007	291.38
7	279	1.59	321.01	0.1023	310.26
8	---	0.82	300.78	0.1039	290.78
9	213	1.28	321.75	0.1040	282.05

Table 2: The sample comparisons shown here are for the case #7 of Table 1.Here $\mathbf{y}(x)$ is the sum of the first three terms on the right side of (48) and $\mathbf{y}'(x) \equiv [y'_1(x), y'_2((x), y'_3(x))]^T$ is the derivative of the three term expansion. The values of $\mathbf{y}_1$, $\mathbf{y}_2$, and $\mathbf{y}_3$ in (48) are respectively $\mathbf{y}_1$=[-0.008511, 0.01332, 0.010639]^T, $\mathbf{y}_2$=[-0.001272, -0.001411, -0.001411]^T, and $\mathbf{y}_3$=[-0.0001209, 0.000115, 0.0000783]^T.The components of $\mathbf{g}$ defined in (45) are evaluated at the above mentioned three term representation for $\mathbf{y}(x)$.

x	$y'_1(x)$	g_1	$y'_2(x)$	g_2	$y'_3(x)$	g_3
0.100E-05	-4.2568	-4.2568	5.3181	5.3782	6.6595	6.7799
0.200E-05	-3.0104	-3.0104	3.7601	3.8026	4.7086	4.7937
0.300E-05	-2.4582	-2.4582	3.0698	3.1045	3.8443	3.9138
0.400E-05	-2.1290	-2.1290	2.6584	2.6884	3.3291	3.3892
0.500E-05	-1.9044	-1.9044	2.3776	2.4044	2.9774	3.0313
0.600E-05	-1.7386	-1.7386	2.1703	2.1948	2.7179	2.7670
0.700E-05	-1.6097	-1.6097	2.0092	2.0319	2.5162	2.5617
0.800E-05	-1.5058	-1.5058	1.8793	1.9006	2.3536	2.3961
0.900E-05	-1.4198	-1.4198	1.7718	1.7918	2.2189	2.2590
0.100E-04	-1.3470	-1.3470	1.6808	1.6998	2.1050	2.1430
0.120E-04	-1.2297	-1.2297	1.5342	1.5516	1.9214	1.9562
0.140E-04	-1.1386	-1.1386	1.4203	1.4364	1.7788	1.8110
0.160E-04	-1.0651	-1.0651	1.3285	1.3435	1.6638	1.6939
0.180E-04	-1.0043	-1.0043	1.2524	1.2666	1.5686	1.5970
0.200E-04	-0.9528	-0.9528	1.1881	1.2015	1.4880	1.5149
0.220E-04	-0.9085	-0.9085	1.1327	1.1455	1.4187	1.4444
0.240E-04	-0.8699	-0.8699	1.0844	1.0967	1.3582	1.3828
0.260E-04	-0.8358	-0.8358	1.0418	1.0536	1.3049	1.3285
0.270E-04	-0.8202	-0.8202	1.0223	1.0339	1.2805	1.3037
0.280E-04	-0.8055	-0.8055	1.0039	1.0153	1.2574	1.2801
0.290E-04	-0.7915	-0.7915	0.9864	0.9976	1.2355	1.2578
0.300E-04	-0.7782	-0.7782	0.9698	0.9808	1.2147	1.2367

Table 3: This table exhibits the validity of the proposed correlation for c_1 in (52).

$\frac{\rho_2}{\rho_1}$	$\frac{\mu_2}{\mu_1}$	Re	$\frac{Ja}{Pr_1}$	c_1 (computed)	c_1 (correlation)	% error in c_1
0.00508	0.01689	9631.03	0.03163	0.03034	0.02948	2.82
0.00490	0.01660	13916.75	0.03112	0.02589	0.02557	1.22
0.00494	0.01657	29978.45	0.03187	0.01887	0.01881	0.34
0.00489	0.01663	36766.67	0.03088	0.01713	0.01719	-0.35
0.00500	0.01689	50131.07	0.03068	0.01496	0.01500	-0.28
0.00508	0.01766	15192.22	0.02637	0.02310	0.02309	0.01
0.00498	0.01746	48001.75	0.02627	0.01438	0.01454	-1.15
0.00481	0.01743	67619.74	0.02412	0.01218	0.01245	-2.20
0.00496	0.01863	14764.91	0.01780	0.02030	0.02076	-2.28
0.00500	0.01859	22680.46	0.01880	0.01735	0.01769	-1.93
0.00494	0.01852	49418.00	0.01836	0.01262	0.01284	-1.75
0.00490	0.01847	70759.56	0.01831	0.01094	0.01111	-1.60
0.00498	0.01970	20152.73	0.00967	0.01505	0.01500	0.37
0.00496	0.01965	27764.10	0.00975	0.01332	0.01322	0.78
0.00502	0.01969	42230.87	0.01046	0.01151	0.01135	1.42
0.00521	0.02005	56968.28	0.01046	0.01023	0.00992	3.03
0.00491	0.01955	64291.90	0.00978	0.00963	0.00943	2.08
0.00483	0.01941	75081.94	0.00963	0.00904	0.00886	2.06
0.00828	0.01959	17242.49	0.04536	0.02592	0.02207	14.85
0.00843	0.01992	39747.77	0.04491	0.01811	0.01556	14.09
0.00815	0.01961	49550.31	0.04376	0.01655	0.01427	13.74
0.00848	0.02114	16889.67	0.03720	0.02381	0.02071	13.02
0.00795	0.02062	33906.02	0.03460	0.01758	0.01557	11.40
0.00833	0.02101	40265.69	0.03641	0.01658	0.01453	12.37
0.00856	0.02135	60914.93	0.03670	0.01400	0.01219	12.92
0.00847	0.02139	90206.66	0.03543	0.01182	0.01031	12.79
0.00825	0.02244	10346.21	0.02525	0.02522	0.02251	10.73
0.00825	0.02246	27589.90	0.02509	0.01699	0.01507	11.29
0.00808	0.02226	55883.58	0.02443	0.01277	0.01129	11.57
0.00814	0.02235	87985.34	0.02442	0.01066	0.00936	12.18

Table 4: Values of coefficients defined in sections 7 and 8

Coefficients dependent on ρ_2/ρ_1 and μ_2/μ_1 as they appear in sections 7 and 8	Fluid: R-113 $\rho_2/\rho_1 \cong 0.005$, and $\mu_2/\mu_1 \cong 0.0185$	Fluid: FC-72 $\rho_2/\rho_1 \cong 0.0082$, and $\mu_2/\mu_1 \cong 0.0185$
a_1	9864.78	12355.3
$\hat{a}_1$	11,154.30	16,822.30
β_{00}	6.5824×10^{9}	6.8758×10^{9}
β_{01}	6.2335×10^{7}	7.9341×10^{7}
Ja_1	0.025	0.026
β_{10}	1.3709×10^{-6}	1.2828×10^{-6}
β_{11}	1.5685×10^{-4}	1.0025×10^{-4}
ε_{00}	$4.0788\text{x}10^{-18}$	$12.9278\text{x}10^{-18}$
ε_{01}	$8.398\text{x}10^{-14}$	$18.3508\text{x}10^{-14}$
ε_{10}	$4.2359\text{x}10^{13}$	$13.0428\text{x}10^{13}$
f_{00}	$1.3724\text{x}10^{9}$	$1.5110\text{x}10^{9}$
f_{01}	$8.9932\text{x}10^{6}$	$11.9523\text{x}10^{6}$
f_{10}	$2.7349\text{x}10^{-7}$	$3.0552\text{x}10^{-7}$
δ_{00}	0.1178	0.1099
δ_{10}	1063.93	1131.66
n_{00}	12.8473	13.7720
n_{10}	0.001503	0.001413
π_{00}	36417.8	65015.2
π_{01}	$7.05327\text{x}10^{6}$	$10.9957\text{x}10^{6}$
π_{10}	$1.6288\text{x}10^{-7}$	$1.1817\text{x}10^{-7}$
π_{11}	$6.1984\text{x}10^{-12}$	$6.5865\text{x}10^{-12}$
u_{00}	10561.3	9278.94
u_{10}	0.04756	0.03691
Coefficients dependent on μ_2/μ_1 alone as they appear in sections 7 and 8	Fluids: R-113 and FC-72. It is assumed that for both the fluids: $\mu_2/\mu_1 \cong 0.02$	
a_{10}	106,776.0	
$\hat{a}_{10}$	861,770.0	

Table 5: The Table below compares the predicted correlations for film thickness and average heat transfer coefficients with sample experimental measurements of Lu [15]. Here $\delta_3 = \Delta(x_3)/h$, where $x_3 = 0.254$ m and h = 0.025 m, and $\bar{h}_2 = \bar{h}_x$ where $x = 0.5993$ m.

Row #	Expt. Run # in [15]	Inlet Speed U (m/ s)	Press. p_0 (MPa)	Temp. $T_s(p_0)$ (K)	Temp. T_w (K)	β (run)	β (fit)	δ_3 Expt.	δ_3 Model	% error in δ_3	$\bar{h}_2$ Expt. (W/ m²-K)	$\bar{h}_2$ Model (W/ m²-K)	% error in $\bar{h}_2$
Fluid: Refrigerant R-113													
1	179	0.53	0.10733	322.47	283.22	26.00	22.91				208.57	203.72	2.33
2	201	0.68	0.10589	322.06	282.27		16.26	0.44200	0.47940	-8.46	230.78	213.84	7.34
3	239	0.79	0.10338	321.33	282.23	9.50	12.91				203.16	221.07	-8.82
4	178	0.85	0.10576	322.02	282.49		11.58				223.68	223.95	-0.12
5	172	1.01	0.10178	320.86	281.41	7.80	9.17				232.20	232.03	0.07
6	177	1.15	0.10273	321.14	282.66		7.26				249.92	239.14	4.31
7	223	1.25	0.10310	321.25	284.22	5.70	6.06				237.55	244.70	-3.01
8	273*	1.27	0.10141	320.75	281.15								
9	194	1.40	0.10765	322.56	282.09								
10	187*	1.50	0.10751	322.52	283.01								
11	190	1.69	0.10423	321.58	281.47	5.70	5.32				274.24	305.84	-11.52
12	205	1.72	0.10530	321.89	282.07	5.60	5.59				280.86	315.21	-12.23
13	281	2.09	0.10320	321.28	282.52	10.30	7.64				387.51	389.96	-0.63
14	242	2.80	0.10537	321.91	284.12	14.30	14.21				519.43	563.14	-8.42
15		0.82	0.10390	300.78	290.78								
16	226	0.72	0.10334	321.32	290.04	9.40	10.80				208.64	225.22	-7.95

(Sheet 1 of 6)

Table 5: (Continued) The Table below compares the predicted correlations for film thickness and average heat transfer coefficients with sample experimental measurements of Lu [15]. Here $\delta_3 = \Delta(x_3)/h$, where $x_3 = 0.254$ m and h = 0.025 m, and $\bar{h}_2 = \bar{h}_x$ where $x = 0.5993$ m.

Row #	Expt. Run # in [15]	Inlet Speed U (m/ s)	Press. p_0 (MPa)	Temp. $T_s(p_0)$ (K)	Temp. T_w (K)	β (run)	β (fit)	δ_3 Expt.	δ_3 Model	% error in δ_3	$\bar{h}_2$ Expt. (W/ m²-K)	$\bar{h}_2$ Model (W/ m²-K)	% error in $\bar{h}_2$
17	184	0.82	0.10389	321.48	290.78	9.40	8.64				224.38	231.98	-3.39
18	207	0.84	0.10670	322.29	290.67	8.50	8.56	0.39700	0.43680	-10.03	217.37	231.82	-6.65
19	196	1.03	0.10300	321.22	290.67	5.50	6.15				220.00	243.16	-10.53
20	214*	1.25	0.10628	322.17	290.92								
21	284	1.32	0.10269	321.13	289.59						256.52		
22	228	1.44	0.10447	321.65	290.55						250.89		
23	193	1.49	0.11082	323.45	292.41						265.52		
24	191	1.59	0.10680	322.32	290.63						272.21		
25	206*	1.73	0.10530	321.89	290.94								
26	247	2.20	0.10074	320.55	290.30	4.80	5.66				346.95	400.83	-15.53
27	237	2.41	0.10043	320.46	290.60		6.65				416.80	445.58	-6.90
28	276	2.70	0.10451	321.66	289.90	10.40	10.02				481.42	530.48	-10.19
29	291	3.12	0.10134	320.73	290.22		11.83				563.97	612.10	-8.53
30	257	3.24	0.10496	321.79	291.56	13.50	13.67				583.85	660.86	-13.19
31	241	3.74	0.10747	322.51	291.57		19.97				667.69	802.02	-20.12
32	234	3.92	0.10077	320.56	291.38	16.00	17.43				707.75	798.63	-12.84
33	231	4.35	0.09937	320.14	289.81		22.07				783.21		
34	221	0.31	0.10786	322.62	301.20	26.60	28.39	0.38700	0.48880	-26.29	203.78	204.07	-0.14

(Sheet 2 of 6)

Table 5: (Continued) The Table below compares the predicted correlations for film thickness and average heat transfer coefficients with sample experimental measurements of Lu [15]. Here $\delta_3 = \Delta(x_3)/h$, where $x_3 = 0.254$ m and h = 0.025 m, and $\bar{h}_2 = \bar{h}_x$ where $x = 0.5993$ m.

Row #	Expt. Run # in [15]	Inlet Speed U (m/ s)	Press. p_0 (MPa)	Temp. $T_s(p_0)$ (K)	Temp. T_w (K)	β (run)	β (fit)	δ_3 Expt.	δ_3 Model	% error in δ_3	$\bar{h}_2$ Expt. (W/ m^2-K)	$\bar{h}_2$ Model (W/ m^2-K)	% error in $\bar{h}_2$
35	181	0.50	0.11043	323.34	301.97		13.53	0.34200	0.44230	-29.33	227.47	225.05	1.06
36	203	0.71	0.10215	320.97	300.86		8.58	0.34400	0.40900	-18.88	235.06	244.53	-4.03
37	185	0.84	0.10310	321.25	300.79	5.70	6.66	0.37000	0.39660	-7.19	225.58	252.08	-11.75
38	126	0.94	0.10472	321.72	303.24		5.31				220.17	263.75	-19.79
39	211	1.12	0.10379	321.45	300.25	5.25	4.38	0.36800	0.37710	-2.48	262.03	265.21	-1.21
40	62	1.15	0.11363	324.22	304.26		3.73	0.36700	0.36720	-0.06	247.37	269.94	-9.12
41	125	1.20	0.10896	322.93	302.23		3.72				256.39	270.25	-5.41
42	215	1.28	0.10409	321.54	299.89	3.20	3.61	0.34500	0.36880	-6.90	248.41	271.28	-9.21
43	286*	1.39	0.10338	321.33	300.73								
44	217	1.48	0.10551	321.95	300.34								
45	218	1.74	0.10825	322.73	301.52								
46	128*	1.90	0.10368	321.42	302.19								
47	248	2.15	0.10195	320.91	300.82	4.10	3.91				366.18	388.51	-6.10
48	262	2.69	0.10063	320.52	299.77		5.37				458.73	502.43	-9.53
49	263	2.82	0.10273	321.14	299.95	5.60	6.03				461.68	541.84	-17.36
50	287	3.13	0.10458	321.68	300.29	8.50	7.21				575.62	624.16	-8.43
51	245	3.74	0.11301	324.05	304.77		9.35				644.63	826.25	-28.17
52	294	4.06	0.10205	320.94	299.76	8.80	9.83				672.99	832.68	-23.73

(Sheet 3 of 6)

Table 5: (Continued) The Table below compares the predicted correlations for film thickness and average heat transfer coefficients with sample experimental measurements of Lu [15]. Here $\delta_3 = \Delta(x_3)/h$, where $x_3 = 0.254$ m and h = 0.025 m, and $\bar{h}_2 = \bar{h}_x$ where $x = 0.5993$ m.

Row #	Expt. Run # in [15]	Inlet Speed U (m/ s)	Press. p_0 (MPa)	Temp. $T_s(p_0)$ (K)	Temp. T_w (K)	β (run)	β (fit)	δ_3 Expt.	δ_3 Model	% error in δ_3	$\bar{h}_2$ Expt. (W/ m²-K)	$\bar{h}_2$ Model (W/ m²-K)	% error in $\bar{h}_2$
53	288	4.34	0.10114	320.67	300.70		10.04				729.68	893.12	-22.40
54	269	1.15	0.10273	321.14	310.50	3.00	3.19				281.33	310.75	-10.46
55	268	1.40	0.09960	320.21	310.24	2.60	2.40				303.32	328.38	-8.26
56	279*	1.59	0.10229	321.01	310.26	1.90						331.00	
57	267	1.85	0.10239	321.04	309.87								
58	249	2.16	0.10249	321.07	309.45								
59	266*	2.19	0.10256	321.09	309.58								
60	265	2.39	0.10375	321.44	309.92	3.10	2.68				445.43	442.99	0.55
61	264	2.95	0.09993	320.31	310.09		2.99				566.85	549.90	2.99
62	258	3.13	0.10754	322.53	311.17	4.00	4.03				552.80	631.63	-14.26
63	272	3.71	0.10134	320.73	309.90	4.50	4.44				646.38	732.86	-13.38
64	295	3.91	0.10344	321.35	309.64		5.32				655.92	795.93	-21.35
65	271	4.17	0.09924	320.10	309.84		4.78				687.29	826.71	-20.29
66	250	4.39	0.09970	320.24	309.53	5.10	5.39				725.49	883.22	-21.74
Fluid: Fluorinert Carbon FC-72													
67	311	0.80	0.10199	331.04	289.92	13.00	11.93	0.4800	0.4306	10.29	175.34	178.92	-2.04
68	312	0.59	0.10199	331.04	290.18	18.00	18.60	0.4840	0.4574	5.49	166.55	168.39	-1.11
69	345*	0.84	0.10102	330.75	290.17	10.00	10.96						

(Sheet 4 of 6)

Table 5: (Continued) The Table below compares the predicted correlations for film thickness and average heat transfer coefficients with sample experimental measurements of Lu [15]. Here $\delta_3 = \Delta(x_3)/h$, where $x_3 = 0.254$ m and h = 0.025 m, and $\bar{h}_2 = \bar{h}_x$ where $x = 0.5993$ m.

Row #	Expt. Run # in [15]	Inlet Speed U (m/ s)	Press. p_0 (MPa)	Temp. $T_s(p_0)$ (K)	Temp. T_w (K)	β (run)	β (fit)	δ_3 Expt.	δ_3 Model	% error in δ_3	$\bar{h}_2$ Expt. (W/ m²-K)	$\bar{h}_2$ Model (W/ m²-K)	% error in $\bar{h}_2$
70	306*	1.34	0.10388	331.60	291.74								
71	368	1.72	0.10020	330.50	291.10	30.00	23.62				393.82	393.10	0.18
72	367	2.15	0.10089	330.71	291.63	46.00	37.42				504.68	516.34	-2.31
73	370	2.45	0.09934	330.24	291.19	46.50	46.96				554.17	595.20	-7.40
74	313	0.57	0.10375	331.56	300.19	11.50	13.69	0.4180	0.4362	-4.36	163.78	174.70	-6.67
75	314	0.84	0.09990	330.41	299.60	6.50	7.63	0.3970	0.4024	-1.36	174.98	189.73	-8.43
76	315*	1.21	0.09681	329.46	299.58								
77	316*	1.38	0.10179	330.98	300.08	8.00	11.37						
78	372	1.83	0.10106	330.76	299.62		20.05				401.37	423.06	-5.40
79	349	2.04	0.10474	331.85	301.17	28.00	26.74				487.02	497.35	-2.12
80	373	2.29	0.09762	329.71	300.16	27.20	27.06				500.52	535.24	-6.94
81	352	2.61	0.09768	329.73	299.96		35.72				554.05	626.34	-13.05
82	378	3.05	0.10351	331.49	301.90	43.00	56.02				683.97	794.96	-16.23
83	346	0.90	0.09758	329.70	300.11	7.00	6.57				194.59	193.91	0.35
84	322	0.36	0.09990	330.41	310.15	14.50	16.82	0.3410	0.4354	-27.70	167.47	173.43	-3.56
85	321	0.51	0.09852	329.99	310.32		10.05	0.3400	0.4033	-18.62	186.25	187.30	-0.56
86	319	0.67	0.10059	330.62	310.15	6.00	6.67	0.3390	0.3848	-13.52	174.16	196.20	-12.65
87	323	0.96	0.09990	330.41	310.29	4.00	3.91	0.3170	0.3565	-12.46	192.50	211.80	-10.02

(Sheet 5 of 6)

Table 5: (Continued) The Table below compares the predicted correlations for film thickness and average heat transfer coefficients with sample experimental measurements of Lu [15]. Here $\delta_3 = \Delta(x_3)/h$, where $x_3 = 0.254$ m and h = 0.025 m, and $\bar{h}_2 = \bar{h}_x$ where $x = 0.5993$ m.

Row #	Expt. Run # in [15]	Inlet Speed U (m/ s)	Press. p_0 (MPa)	Temp. $T_s(p_0)$ (K)	Temp. T_w (K)	β (run)	β (fit)	δ_3 Expt.	δ_3 Model	% error in δ_3	$\bar{h}_2$ Expt. (W/ m^2-K)	$\bar{h}_2$ Model (W/ m^2-K)	% error in $\bar{h}_2$
88	325*	1.27	0.10096	330.73	310.74								
89	358	1.98	0.09768	329.73	309.98	8.00	11.32				363.40	445.57	-22.61
90	359	2.33	0.09784	329.78	309.69	18.50	16.23				510.55	542.28	-6.21
91	379	2.85	0.10139	330.86	310.06	19.50	28.06				582.67	712.98	-22.36
92	361	3.10	0.09836	329.94	310.27	38.50	28.48				781.68	766.22	1.98
93	331	0.69	0.10010	330.47	319.94	5.00	4.89	0.2700	0.3269	-21.08	195.44	228.66	-17.00
94	338*	1.61		331.47	320.86								
95	390	2.01		329.97	320.25	3.00	3.21				351.22	452.17	-28.74
96	340	2.15		331.05	320.66	3.85	3.98				384.08	506.40	-31.85
97	341	2.52		330.21	320.31	3.90	4.51				424.79	596.88	-40.51
98	384	2.78		330.71	320.36	6.45	5.54				525.57	681.58	-29.68

(Sheet 6 of 6)

Recent IMA Preprints

#	Author/s	Title
1021	**IMA Summer Program for Graduate Students**,	Mathematical Modeling
1022	**Wayne Barrett, Charles R. Johnson, and Pablo Tarazaga**,	The real positive definite completion problem for a simple cycle
1023	**Charles A. McCarthy**,	Fourth order accuracy for a cubic spline collocation method
1024	**Martin Hanke, James Nagy, and Robert Plemmons**,	Preconditioned iterative regularization for I11-posed problems
1025	**John R. Gilbert, Esmond G. Ng, and Barry W. Peyton**,	An efficient algorithm to compute row and column counts for sparse Cholesky factorization
1026	**Xinfu Chen**,	Existence and regularity of solutions of a nonlinear nonuniformly elliptic system arising from a thermistor problem
1027	**Xinfu Chen and Weiqing Xie**,	Discontinuous solutions of steady state, viscous compressible Navier-Stokes equations
1028	**E.G. Kalnins, Willard Miller, Jr., and Sanchita Mukherjee**,	Models of q-algebra representations: Matrix elements of the q-oscillator algebra
1029	**W. Miller, Jr. and Lee A. Rubel**,	Functional separation of variables for Laplace equations in two dimensions
1030	**I. Gohberg and I. Koltracht**,	Structured condition numbers for linear matrix structures
1031	**Xinfu Chen**,	Hele-Shaw problem and area preserved curve shortening motion
1032	**Zhangxin Chen and Jim Douglas, Jr.**	Modelling of compositional flow in naturally fractured reservoirs
1033	**Harald K. Wimmer**,	On the existence of a least and negative-semidefinite solution of the discrete-time algebraic Riccati equation
1034	**Harald K. Wimmer**,	Monotonicity and parametrization results for continuous-time algebraic Riccati equations and Riccati inequalities
1035	**Bart De Moor, Peter Van Overschee, and Geert Schelfhout**,	H_2 model reduction for SISO systems
1036	**Bart De Moor**,	Structured total least squares and L_2 approximation problems
1037	**Chjan Lim**,	Nonexistence of Lyapunov functions and the instability of the Von Karman vortex streets
1038	**David C. Dobson and Fadil Santosa**,	Resolution and stability analysis of an inverse problem in electrical impedance tomography – dependence on the input current patterns
1039	**C.N. Dawson, C.J. van Duijn, and M.F. Wheeler**,	Characteristic-Galerkin methods for contaminant transport with non-equilibrium adsorption kinetics
1040	**Bing-Yu Zhang**,	Analyticity of solutions of the generalized Korteweg-de Vries equation with respect to their initial values
1041	**Neerchal K. Nagaraj and Wayne A. Fuller**,	Least squares estimation of the linear model with autoregressive errors
1042	**H.J. Sussmann & W. Liu**,	A characterization of continuous dependence of trajectories with respect to the input for control-affine systems
1043	**Karen Rudie & W. Murray Wonham**,	Protocol verification using discrete-event systems
1044	**Rohan Abeyaratne & James K. Knowles**,	Nucleation, kinetics and admissibility criteria for propagating phase boundaries
1045	**Gang Bao & William W. Symes**,	Computation of pseudo-differential operators
1046	**Srdjan Stojanovic**,	Nonsmooth analysis and shape optimization in flow problem
1047	**Miroslav Tuma**,	Row ordering in sparse QR decomposition
1048	**Onur Toker & Hitay Özbay**,	On the computation of suboptimal H^∞ controllers for unstable infinite dimensional systems
1049	**Hitay Özbay**,	H^∞ optimal controller design for a class of distributed parameter systems
1050	**J.E. Dunn & Roger Fosdick**,	The Weierstrass condition for a special class of elastic materials
1051	**Bei Hu & Jianhua Zhang**,	A free boundary problem arising in the modeling of internal oxidation of binary alloys
1052	**Eduard Feireisl & Enrique Zuazua**,	Global attractors for semilinear wave equations with locally distributed nonlinear damping and critical exponent
1053	**I-Heng McComb & Chjan C. Lim**,	Stability of equilibria for a class of time-reversible, $D_n x O(2)$-symmetric homogeneous vector fields
1054	**Ruben D. Spies**,	A state-space approach to a one-dimensional mathematical model for the dynamics of phase transitions in pseudoelastic materials
1055	**H.S. Dumas, F. Golse, and P. Lochak**,	Multiphase averaging for generalized flows on manifolds
1056	**Bei Hu & Hong-Ming Yin**,	Global solutions and quenching to a class of quasilinear parabolic equations
1057	**Zhangxin Chen**,	Projection finite element methods for semiconductor device equations
1058	**Peter Guttorp**,	Statistical analysis of biological monitoring data
1059	**Wensheng Liu & Héctor J. Sussmann**,	Abnormal sub-Riemannian minimizers

1060 **Chjan C. Lim**, A combinatorial perturbation method and Arnold's whiskered Tori in vortex dynamics
1061 **Yong Liu**, Axially symmetric jet flows arising from high speed fiber coating
1062 **Li Qiu & Tongwen Chen**, $\mathcal{H}_2$ and $\mathcal{H}_\infty$ designs of multirate sampled-data systems
1063 **Eduardo Casas & Jiongmin Yong**, Maximum principle for state-constrained optimal control problems covered by quasilinear elliptic equations
1064 **Suzanne M. Lenhart & Jiongmin Yong**, Optimal control for degenerate parabolic equations with logistic growth
1065 **Suzanne Lenhart**, Optimal control of a convective-diffusive fluid problem
1066 **Enrique Zuazua**, Weakly nonlinear large time behavior in scalar convection-diffusion equations
1067 **Caroline Fabre, Jean-Pierre Puel & Enrike Zuazua**, Approximate controllability of the semilinear heat equation
1068 **M. Escobedo, J.L. Vazquez & Enrike Zuazua**, Entropy solutions for diffusion-convection equations with partial diffusivity
1069 **M. Escobedo, J.L. Vazquez & Enrike Zuazua**, A diffusion-convection equation in several space dimensions
1070 **F. Fagnani & J.C. Willems**, Symmetries of differential systems
1071 **Zhangxin Chen, Bernardo Cockburn, Joseph W. Jerome & Chi-Wang Shu**, Mixed-RKDG finite element methods for the 2-D hydrodynamic model for semiconductor device simulation
1072 **M.E. Bradley & Suzanne Lenhart**, Bilinear optimal control of a Kirchhoff plate
1073 **Héctor J. Sussmann**, A cornucopia of abnormal subriemannian minimizers. Part I: The four-dimensional case
1074 **Marek Rakowski**, Transfer function approach to disturbance decoupling problem
1075 **Yuncheng You**, Optimal control of Ginzburg-Landau equation for superconductivity
1076 **Yuncheng You**, Global dynamics of dissipative modified Korteweg-de Vries equations
1077 **Mario Taboada & Yuncheng You**, Nonuniformly attracting inertial manifolds and stabilization of beam equations with structural and Balakrishnan-Taylor damping
1078 **Michael Böhm & Mario Taboada**, Global existence and regularity of solutions of the nonlinear string equation
1079 **Zhangxin Chen**, BDM mixed methods for a nonlinear elliptic problem
1080 **J.J.L. Velázquez**, On the dynamics of a closed thermosyphon
1081 **Frédéric Bonnans & Eduardo Casas**, Some stability concepts and their applications in optimal control problems
1082 **Hong-Ming Yin**, $\mathcal{L}^{2,\mu}(Q)$-estimates for parabolic equations and applications
1083 **David L. Russell & Bing-Yu Zhang**, Smoothing and decay properties of solutions of the Korteweg-de Vries equation on a periodic domain with point dissipation
1084 **J.E. Dunn & K.R. Rajagopal**, Fluids of differential type: Critical review and thermodynamic analysis
1085 **Mary Elizabeth Bradley & Mary Ann Horn**, Global stabilization of the von Kármán plate with boundary feedback acting via bending moments only
1086 **Mary Ann Horn & Irena Lasiecka**, Global stabilization of a dynamic von Kármán plate with nonlinear boundary feedback
1087 **Vilmos Komornik**, Decay estimates for a petrovski system with a nonlinear distributed feedback
1088 **Jesse L. Barlow**, Perturbation results for nearly uncoupled Markov chains with applications to iterative methods
1089 **Jong-Shenq Guo**, Large time behavior of solutions of a fast diffusion equation with source
1090 **Tongwen Chen & Li Qiu**, $\mathcal{H}_\infty$ design of general multirate sampled-data control systems
1091 **Satyanad Kichenassamy & Walter Littman**, Blow-up surfaces for nonlinear wave equations, I
1092 **Nahum Shimkin**, Asymptotically efficient adaptive strategies in repeated games, Part I: certainty equivalence strategies
1093 **Caroline Fabre, Jean-Pierre Puel & Enrique Zuazua**, On the density of the range of the semigroup for semilinear heat equations
1094 **Robert F. Stengel, Laura R. Ray & Christopher I. Marrison**, Probabilistic evaluation of control system robustness
1095 **H.O. Fattorini & S.S. Sritharan**, Optimal chattering controls for viscous flow
1096 **Kathryn E. Lenz**, Properties of certain optimal weighted sensitivity and weighted mixed sensitivity designs
1097 **Gang Bao & David C. Dobson**, Second harmonic generation in nonlinear optical films
1098 **Avner Friedman & Chaocheng Huang**, Diffusion in network
1099 **Xinfu Chen, Avner Friedman & Tsuyoshi Kimura**, Nonstationary filtration in partially saturated porous media
1100 **Walter Littman & Baisheng Yan**, Rellich type decay theorems for equations $P(D)u = f$ with f having support in a cylinder
1101 **Satyanad Kichenassamy & Walter Littman**, Blow-up surfaces for nonlinear wave equations, II
1102 **Nahum Shimkin**, Extremal large deviations in controlled I.I.D. processes with applications to hypothesis testing
1103 **A. Narain**, Interfacial shear modeling and flow predictions for internal flows of pure vapor experiencing film condensation
1104 **Andrew Teal & Laurent Praly**, Global stabilizability and observability imply semi-global stabilizability by output feedback